Carbenoxolone and 18β-Glycyrrhetinic Acid Inhibit IP_3-Mediated Endothelial Cell Calcium Signalling and Depolarise Mitochondria

Charlotte Buckley, Xun Zhang, Calum Wilson & John G. McCarron

Strathclyde Institute of Pharmacy and Biomedical Sciences, University of Strathclyde, 161 Cathedral Street, Glasgow G4 0RE, UK.

Short title: Gap junction blockers inhibit IP_3 receptors and mitochondria

Total word count: 4182

Keywords:
Vascular, endothelium, calcium, gap junctions, inositol 1,4,5-trisphosphate (IP_3), mitochondria, Carbenoxolone and 18β-Glycyrrhetinic Acid

Correspondence: John G McCarron (john.mccarron@strath.ac.uk), Strathclyde Institute of Pharmacy and Biomedical, University of Strathclyde, 161 Cathedral Street, Glasgow, G4 0RE, UK.

Abstract

Background and Purpose Coordinated endothelial control of cardiovascular function is proposed to occur by endothelial cell communication via gap junctions and connexins. To study intercellular communication, the pharmacological agents carbenoxolone (CBX) and 18β glycyrrhetinic acid (18βGA) are used widely as connexin inhibitors and gap junction blockers.

Experimental Approach We investigated the effects of CBX and 18βGA on IP_3-evoked intercellular Ca^{2+} waves in the endothelium of intact mesenteric resistance arteries.

Key Results Acetylcholine (ACh)-evoked IP_3-mediated Ca^{2+} release and propagated waves were inhibited by CBX (100μM) and 18βGA (40μM). Unexpectedly, the Ca^{2+} signals were inhibited uniformly in all cells, suggesting that CBX and 18βGA reduced Ca^{2+} release. Localised photolysis of caged IP_3 (cIP_3) was used to provide precise spatiotemporal control of site of cell activation. Local cIP_3 photolysis generated reproducible Ca^{2+} increases and Ca^{2+} waves that propagated across cells distant to the photolysis site. CBX and 18βGA each blocked Ca^{2+} waves in a time dependent manner by inhibiting the initiating IP_3-evoked Ca^{2+} release event rather than block of gap junctions. This effect was reversed on drug washout, and was unaffected by small or intermediate K^+-channel blockers. Furthermore, CBX and 18βGA each rapidly and reversibly collapsed the mitochondrial membrane potential.

Conclusion and Implications CBX and 18βGA inhibit IP_3-mediated Ca^{2+} release and depolarise the mitochondrial membrane potential. These results suggest that CBX and 18βGA block cell-cell communication by acting at sites that are unrelated to gap junctions.

What is already known

- Cell-cell communication is central to endothelial control of cardiovascular function
- CBX and 18βGA are putative connexin inhibitors and gap junction blockers.
- CBX and 18βGA are widely used to determine mechanisms underlying cell-cell communication.

What this study adds

- CBX and 18βGA inhibit IP_3-evoked Ca^{2+} release
- CBX and 18βGA collapse the mitochondrial membrane potential

Clinical significance

- CBX and 18βGA exert control of cell-cell communication by acting at sites that are unrelated to gap junctions.

Introduction

Cell-cell communication is a central component of endothelial function that is required for propagated vasodilation, transfer of signals from activated cells and emergent signalling (Bagher & Segal, 2011; Lee, Wilson, Saunter, Kennedy, Girkin & McCarron, 2018; Longden et al., 2017; McCarron, Wilson, Heathcote, Zhang, Buckley & Lee, 2019; Socha, Domeier, Behringer & Segal, 2012; Tallini et al., 2007). Among key signalling molecules that are transferred between cells are IP_3 and cytoplasmic Ca^{2+}. Changes in IP_3 and cytoplasmic Ca^{2+} concentration decode information held in extracellular activators and encode intracellular signals that regulate the production of nitric oxide, prostacyclin, and signalling peptides that diffuse to smooth muscle cells (Tran & Watanabe, 2006).

In the endothelium, Ca^{2+} increases begin as highly localized subcellular events caused by the opening of a single or multiple IP_3 receptors (IP_3Rs) in the internal store (Bagher, Beleznai, Kansui, Mitchell, Garland & Dora, 2012; Ledoux et al., 2008; Sonkusare et al., 2012; Wilson et al., 2019). These local signals rapidly grow and propagate among cells to transmit information. However, the mechanisms that scale the signals to propagate waves and enable cell-cell communication are not well understood even though they are critical to permit Ca^{2+} to act as a communicator with wide reach (Behringer & Segal, 2012; Billaud, Lohman, Johnstone, Biwer, Mutchler & Isakson, 2014; Emerson & Segal, 2000a; Emerson & Segal, 2000b; Ledoux et al., 2008; Sonkusare et al., 2012; Taylor & Francis, 2014).

Several reports describe a central role for specialized intercellular connections (gap junctions) in facilitating cell-cell communication and the transmission of Ca^{2+} signals in endothelial cells (Boittin, Alonso, Le Gal, Allagnat, Beny & Haefliger, 2013; Kameritsch, Pogoda, Ritter, Munzing & Pohl, 2012). Gap junctions operate via membrane-bound connexin hexamers that pair with connexins on adjacent cells (Bai, Yue & Aoyama, 2018). The paired connexins form functional junctions between the membranes through which the cytoplasm of each cell may be linked (reviewed in Saez, Berthoud, Branes, Martinez & Beyer, 2003). The connection permits intercellular movement of ions, e.g. Ca^{2+}, and small molecules with a mass of up to ~1.2kDa, such as ATP (Goldberg, Moreno & Lampe, 2002), cAMP, IP_3 (Hernandez et al., 2007) or ROS (Billaud, Marthan, Savineau & Guibert, 2009; Taniguchi Ishikawa et al., 2012).

Amongst the most widely used pharmacological agents to study the role of gap junctions in cell-cell communication are the connexin and gap junction blockers 18β Glycyrrhetinic Acid

(18βGA) and its derivative carbenoxolone (CBX). Derived from the liquorice root Glycyrrhiza glabra, 18βGA (reviewed in Bodendiek & Raman, 2010) blocks a wide range connexins such as Cx43 (Guan, Wilson, Schlender & Ruch, 1996), Cx46 and Cx50 (Bruzzone, Barbe, Jakob & Monyer, 2005). CBX is a derivative of 18βGA and is perhaps the most widely used broad-spectrum connexin channel and gap junction inhibitor.

To investigate whether or not gap junctions play a role in endothelial IP_3-mediated Ca^{2+} signal propagation between cells, we aimed to disrupt normal gap junction function pharmacologically using CBX and 18βGA. IP_3-evoked intercellular Ca^{2+} waves were measured in the endothelium of intact mesenteric resistance arteries after stimulation with either acetylcholine (ACh) or photorelease of caged-IP_3 (cIP_3). cIP_3 provides precise spatial and temporal control of the site of cell activation and Ca^{2+} release. Paired cellular responses to ACh or cIP_3 were analysed before and after various pharmacological interventions with CBX and 18βGA. Intercellular Ca^{2+} waves were blocked by CBX and 18βGA, but this occurred by inhibition of IP_3-evoked Ca^{2+} release rather than block of gap junction-mediated signal propagation. The inhibition of IP_3-evoked Ca^{2+} release by CBX and 18βGA was reversible, and was unaffected by the presence of small or intermediate K^+-channel blockers. Furthermore, CBX and 18βGA each also rapidly and reversibly collapsed the mitochondrial membrane potential. These results suggest that CBX and 18βGA block cell-cell communication by inhibiting IP_3-mediated Ca^{2+} release and depolarising mitochondrial membrane potential ($\Delta\Psi_M$) rather than acting as classical gap junction blockers.

Methods

Animals

All animal husbandry and euthanasia were carried out in accordance with the prior approval of the University of Strathclyde Animal Welfare and Ethical Review Body and under relevant UK Home Office Regulations, [Schedule 1 of the Animals (Scientific Procedures) Act 1986, UK]. Studies are reported in compliance with the ARRIVE guidelines (McGrath & Lilley, 2015). Strathclyde BPU is a conventional unit which undertakes FELASA quarterly heath monitoring. Male Sprague-Dawley rats (10-12 week old; 250 - 300 g), from an in-house colony, were used for the study. The animals were housed 3 per cage and the cage type was North Kent Plastic model RC2F with nesting material 'Sizzle Nest'. A 12:12 light dark cycle was used with a temperature range of 19 – 23°C (set point 21°C) and humidity levels between 45-65%. Animals had free access to fresh water and SDS diet RM1 (rodent maintenance). The enrichment in the cages was aspen wood chew sticks and hanging huts. Animals were euthanized by cervical dislocation and the mesenteric bed removed. All experiments were performed using first- or second-order mesenteric arteries. Controls and experimental treatments were carried out in the same tissue, so blinding and randomisation were not used.

Mesenteric Artery Preparation and Mounting

Arteries were dissected, cut open longitudinally and pinned out on Sylgard blocks using 50 μm diameter pins to expose the endothelial layer (Lee, Wilson, Saunter, Kennedy, Girkin & McCarron, 2018; Wilson, Lee & McCarron, 2016b). Arteries were dissected in a physiological saline solution (PSS: 145 mM NaCl, 2 mM MOPS, 4.7 mM KCl, 1.2 mM NaH2PO4, 5 mM Glucose, 0.02 mM EDTA, 1.17 mM MgCl, 2 mM CaCl, pH 7.4). PSS or a high K^+ PSS (composition below) was used in all experiments. Endothelial cells were loaded with the Ca^{2+} indicator dye Cal-520 (5 μM in PSS + 0.02% Pluronic F-127, 30 mins, 37^{o}C) and then mounted in a custom flow chamber (Wilson, Lee & McCarron, 2016b).

Image Acquisition

Two imaging systems were used. The first was a Nikon Eclipse TE300 inverted microscope fitted with a CoolLED pE-300 LED illumination system (488 nm and 561 nm excitation) and custom designed, dual FITC/TRITC filter sets (Figure 1A). A 40X 1.3 NA Nikon S Fluor oil-immersion objective lens was used for Ca^{2+} imaging experiments, whilst a 100X 1.3NA

Nikon S-Fluor lens was used in experiments imaging mitochondrial membrane potential. The second imaging system was a Nikon Eclipse FNI upright microscope equipped with a Nikon Fluor 40X 0.8 NA water immersion objective lens and a pE-4000 CoolLED system (470 nm). This system was used for K^+-channel blocking experiments. All images were acquired by Andor iXon EMCCD cameras (1024 x 1024) using MicroManager v1.4.22 (Edelstein, Tsuchida, Amodaj, Pinkard, Vale & Stuurman, 2014).

Localised IP_3 Uncaging

In experiments in which endothelial Ca^{2+} responses were evoked by photolysis of caged IP_3 the endothelium was dual loaded with Cal-520/AM and with a membrane-permeant Ins(1,4,5)P3-caged IP_3 (5 μM; cIP_3; SiChem)(30 mins at 37^{o}C) (Buckley, Wilson & McCarron, 2019; McCarron, Chalmers, MacMillan & Olson, 2010; McCarron & Olson, 2008). Photolysis of cIP_3 was achieved using a Rapp Optoelectronics flash lamp (00-325-JML-C2) at 200 V, which produced light of ~1 ms duration. The flashlamp output was passed through a 395 nm short pass filter into a 1250 μm diameter light guide (Figure 3A). The light-guide was coupled to the epi-illuminator of the TE300 microscope, and the output was focussed on the endothelium using broadband light. For each imaging session, broadband light was used to identify the position of the uncaging region (~ 70 μm diameter) and determine which endothelial cells were directly activated by the spot photolysis system.

In some experiments, the extent of IP_3 uncaging was graded by attenuating the photolysis light power using neutral density filters placed in the excitation path. The neutral density filters had optical densities of 0.5 (27% transmission at 395 nm; product code NE505B; Thor Labs, UK), 0.2 (63% transmission at 395 nm; NE502B; Thor Labs, UK) or 0.1 (80% transmission at 395 nm; NE501B; Thor Labs, UK). These experiments were performed such that the 27% transmission was recorded first, followed by 63% transmission with 15 mins rest between photolysis events, and so on.

Experimental Protocols

In experiments that examined the effect of CBX and 18βGA on IP_3-mediated Ca^{2+} release, ACh- or cIP_3-evoked endothelial Ca^{2+} activity was measured at 10 Hz. Baseline Ca^{2+} activity was recorded for 30 seconds, and then endothelial Ca^{2+} activity evoked by ACh (50 nM) or photolysis of cIP_3. The same arteries were then incubated with CBX (100 μM, 5mins), or 18βGA (40 μM, 45 mins). ACh/cIP_3-evoked Ca^{2+} activity was then recorded again. In

separate experiments, this protocol was repeated with an additional washout period of 1hr (PSS, 1.5 ml.min^{-1}) before an additional recording was taken.

In experiments assessing the effect of K^+-channel blockade on endothelial Ca^{2+} signalling, ACh-evoked (50 nM) Ca^{2+} activity was assessed in the absence and then presence of either apamin (100 nM, 10 min pre-incubation) or TRAM-34 (1 μM; 10 min pre-incubation). After their introduction, antagonists remained in the PSS until washout as indicated. In all experiments there was a minimum of 15 minutes between successive stimulations for responses to recover.

Endothelial cell mitochondrial membrane potential ($\Delta\Psi_M$) was assessed using the membrane potential sensitive fluorophore, tetramethylrhodamine ethyl ester (TMRE; 120 nM in PSS) (Wilson et al., 2019; Zhang, Lee, Wilson & McCarron, 2019). Arteries were incubated in PSS containing TMRE for 10 min. Subsequently, TMRE (120 nM) was continuously present in all perfusion solutions. Images of TMRE fluorescence (excited at 555 nm) were acquired at 2 Hz for 5 mins, with either CBX (100 μM in 120 nM TMRE) or 18βGA (40 μM in 120 nM TMRE) added after ~ 1 min baseline recording.

In a separate series experiments, the effects of CBX and 18βGA on $\Delta\Psi_M$ were investigated whilst changes in the plasma membrane potential were prevented. In these experiments a High-K^+/Ca^{2+}-free PSS (79.7 mM NaCl, 2 mM MOPS, 70 mM KCl, 1.2 mM NaH_2PO_4, 5 mM Glucose, 0.02 mM EDTA, 2 mM NaPy, 1 mM MgCl, 1mM EGTA) was used to prevent plasma membrane potential changes.

In experiments where cell viability was being assessed, propidium iodide (1.5 μM) was added into the PSS, 100 images were acquired and an average image intensity projection generated using Fiji (Schindelin et al., 2012). Propidium iodide was then washed out (10 mins) with PSS and the experiment continued.

Ca^{2+} Signal Analysis

Single-cell Ca^{2+} signals were extracted from Ca^{2+} imaging data as previously described (Wilson, Lee & McCarron, 2016a). In brief, automated Fiji macros were used to extract cell coordinates and track cell positions between datasets. Single-cell Ca^{2+} signals were then extracted and processed using a custom algorithm written in the Python programming language (Wilson, Lee & McCarron, 2016a; Wilson, Saunter, Girkin & McCarron, 2015; Wilson, Saunter, Girkin & McCarron, 2016). Raw fluorescence (*F*) signals were converted to

baseline-corrected fluorescence intensity (F/F_0) by dividing each intensity measurement by the average value of a 100-frame baseline period at the start of each trace. F/F_0 signals were smoothed using a 21-point third order polynomial Savitzky-Golay filter, and key signal parameters (e.g. amplitude, frequency, number of cells, time of event) extracted automatically. Analysis of cIP_3-evoked Ca^{2+} activity was restricted to those cells in which cIP_3 was photolysed. This was achieved by applying a mask restricted to the photolysis region. The photolysis region occupied a fraction of the overall field, so these experiments had a lower number of cells per experiment than those of ACh-evoked signalling.

To visualize Ca^{2+} wave propagation, we created images of active Ca^{2+} wavefronts by calculating $\Delta F/F_0$ for each image in the recording. For cIP_3-evoked Ca^{2+} experiments, a maximum intensity projection of the first 3 images immediately following uncaging was taken, ensuring that only signal from the uncaging area is presented. This only differs in Figure 5, where a maximum intensity projection of the first 5s immediately following uncaging is presented for each experimental condition to compare propagation extent. For ACh experiments, a maximum intensity projection of the 60s after ACh onset was taken. A JET LUT was then applied to the images. Since all experiments were paired, images were contrast matched for control and treatment. To visualise mitochondria, images were loaded into FIJI and an unsharp mask applied, the background subtracted, a Gaussian blur applied and the local contrast enhanced. To get a fluorescence intensity trace, images were stabilised and a region of interest placed over the mitochondria of interest.

Drugs and solutions

Ins(1,4,5)P3-caged IP_3 was obtained from SiChem. Cal-520/AM and TMRE were obtained from Abcam (Cambridge, MA, USA). Pluronic F-127 was obtained from Invitrogen (Carlsbad, CA, USA). TRAM-34 and apamin were obtained from Tocris (Bristol, UK). Carbenoxolone and 18β-glycyrrhetinic acid, ionomycin, acetylcholine, propidium iodide, and all other chemicals were obtained from Sigma (St Louis, MO, USA). All solutions were freshly prepared each day.

Data Availability

All data underpinning this study is available from the authors upon reasonable request.

Statistical Analysis

Graphical summary data represents averaged, paired responses in arteries from ≥5 different animals. Data is summarised as mean ± SEM. Raw peak F/F_0 responses were analysed statistically using either a paired Student's t-test or a paired one-way ANOVA with Tukey's multiple comparisons test on Prism, version 6.0 (GraphPad, La Jolla, CA, USA). $p < 0.05$ was considered statistically significant.

Results

In the endothelium, muscarinic receptor stimulation, using the physiological agonist ACh (50 nM), evoked heterogeneous increases in Ca^{2+}. The Ca^{2+} rise propagated re-generatively, initially within and subsequently between cells, to generate multicellular Ca^{2+} waves (Fig. 1A-B, Supplementary Video 1). These Ca^{2+} waves are the result of IP_3-dependent Ca^{2+} release from intracellular stores (Buckley, Wilson & McCarron, 2020; Wilson, Zhang, Buckley, Heathcote, Lee & McCarron, 2019). In control experiments, repeated application of ACh evoked reproducible increases in Ca^{2+} and propagating waves (Fig 1C-D). There was no difference in the number of cells (306 ± 25 cells for repeat 1, 311 ± 16 cells for repeat 2, n = 5; p = 0.7) or the amplitude of responses (0.26 ± 0.04 $\Delta F/F_0$ for repeat 1, 0.26 ± 0.05 $\Delta F/F_0$ for repeat 2; n = 5; p = 0.9) on each activation with ACh.

It is unclear how these waves are transmitted between neighbouring endothelial cells. A prime candidate for the transmission is the movement of small molecules such as Ca^{2+} or IP_3 through gap junctions between endothelial cells (Pohl, 2020). To explore the role of gap junctions in the intercellular propagation of Ca^{2+} waves, we examined the effects of the two widely used putative gap junction blockers, carbenoxolone (CBX) and 18β-glycyrrhetinic acid (18βGA), on ACh-evoked endothelial cell Ca^{2+} signalling (Figure 2). The expectation in these experiments was that the drugs would reduce transmission of signals without altering the initial Ca^{2+} increase in ACh-activated cells.

CBX (100 μM) and 18βGA (40 μM) each significantly reduced the number of cells responding to ACh (Fig 2A,C)(316 ± 36 cells for control vs 93 ± 60 cells for CBX, Figure 2B; 349 ± 27 cells for control, 129 ± 64 cells for 18βGA, Figure 2D; n = 5 for each; $p < 0.05$) and the amplitude of ACh-evoked responses (0.29 ± 0.08 $\Delta F/F_0$ for control, 0.04 ± 0.03 $\Delta F/F_0$ for CBX, Figure2B; 0.29 ± 0.05 $\Delta F/F_0$ for control, 0.04 ± 0.02 $\Delta F/F_0$ for 18βGA, Figure 2D; n = 5 for each; $p < 0.05$).

These results initially appeared to be consistent with a contribution of gap junctions to the propagation of endothelial cell Ca^{2+} waves. However, the decrease in amplitude of ACh-evoked Ca^{2+} signals occurred approximately uniformly across all endothelial cells – an unexpected finding, as these drugs would not be expected to reduce Ca^{2+} signals in cells directly activated by ACh. Thus, these results suggest that CBX and 18βGA may each directly inhibit IP_3-evoked Ca^{2+} release.

To determine if CBX and 18βGA interfere with the ability of IP_3 to evoke Ca^{2+} release, the effects of the drugs on Ca^{2+} signals evoked by the photolysis of cIP_3 were examined (Figure 4). Uncaged IP_3 bypasses plasma membrane receptors to directly activate IP_3Rs. Photolysis of cIP_3, in a 70 μm diameter spot, triggered an immediate rise in Ca^{2+} in the photolysis region followed by multicellular Ca^{2+} waves that propagated across cells away from the photolysis spot (Figure 3A-B, Supplementary Video 2). The propagating waves encompassed the majority of the cells within the field of view (~330 μm width) by recruiting cells that had not been directly activated by photolysis of caged IP_3 (Fig 2B; Supplementary Video 2). The Ca^{2+} rise evoked by photolysis of cIP_3 was reproducible on repeat activation. In cells within the photolysis spot (Figure 3C-D) there with no difference in either the number of cells activated by cIP_3 (24 ± 1 cells for repeat 1, 24 ± 1 cells for repeat 2, n = 5) or the amplitude of cIP_3-evoked responses (0.80 ± 0.10 $\Delta F/F_0$ for repeat 1, 0.67 ± 0.05 $\Delta F/F_0$ for repeat 2; n = 5; p = 0.2).

CBX and 18βGA each decreased the extent of cIP_3-evoked Ca^{2+} wave propagation (Figure 4, Supplementary Movies 3, 4). However, CBX and 18βGA each also significantly inhibited Ca^{2+} activity evoked in cells directly activated by photolysis of cIP_3 (i.e. Ca^{2+} activity in cells within the photolysis region, Figure 4; Supplementary Movies 3, 4). 18βGA and CBX decreased the amplitude of cIP_3-evoked responses in those cells directly activated by cIP_3 photolysis (0.61 ± 0.04 $\Delta F/F_0$ for control, 0.12 ± 0.03 $\Delta F/F_0$ for CBX, Figure 4B; 0.70 ± 0.03 $\Delta F/F_0$ for control, 0.06 ± 0.04 $\Delta F/F_0$ for 18βGA, Figure 4D; n = 5 for each; $p < 0.05$). 18βGA, but not CBX, also reduced the percentage of cells directly activated by cIP_3 photolysis (21 ± 1 cells for control vs 15 ± 3 cells for CBX, p = 0.13; 21 ± 1 cells for control vs 8 ± 4 cells for 18βGA, $p < 0.05$; n = 5 for each). This result suggests that CBX and 18βGA each have a direct inhibitory action on IP_3Rs.

To determine if CBX and 18βGA inhibition arose *solely* from a direct block of IP_3-evoked Ca^{2+} release, or if inhibition of gap junctions also contributed to the decreased Ca^{2+} response, we examined the time course of the 18βGA-evoked reduction in cIP_3-evoked Ca^{2+} release. IP_3-evoked Ca^{2+} responses were recorded 10 mins before 18βGA incubation (labelled 0 mins; Figure 5A), and then at 15 minute intervals (15 mins were required for Ca^{2+} stores to replenish after photolysis of cIP_3). This experimental protocol was not performed for CBX as the drug's inhibition of Ca^{2+} signalling was too rapid (<10 mins). 18βGA-evoked a time-dependent reduction in: 1) the amplitude of cIP_3-evoked Ca^{2+} signals within the photolysis

site; and 2) the outward propagation of Ca^{2+} signals from the photolysis site (Figure 5A&C). This result raises the possibility that the 18βGA-mediated decrease in outward propagation of Ca^{2+} signals away from the photolysis site may arise from an inhibition of Ca^{2+} release rather than an inhibition of gap junction-mediated communication.

To examine this possibility, we investigated the relationship between the extent of outward propagation of Ca^{2+} waves and the magnitude of initiating cIP_3-evoked Ca^{2+} release. The magnitude of Ca^{2+} release, initiated by the uncaging of cIP_3, was scaled by the control of the photolysis light intensity. As the photolysis light intensity was attenuated, there was a reduction in the amplitude of the Ca^{2+} response in the photolysis site and in the subsequent outward propagation of Ca^{2+} waves (Figure 5B). The relationships between the power of the photolysis stimuli and both the resulting amplitude of cIP_3-evoked Ca^{2+} response and the outward propagation of the Ca^{2+} signal were linear (Figure 5B-C). These results show that the initial Ca^{2+} signal amplitude and the outward propagation of the Ca^{2+} signal are proportional.

Significantly, the magnitude of initiating cIP_3-evoked Ca^{2+} release at various photolysis light transmission percentages plotted against magnitude of initiating cIP_3-evoked Ca^{2+} release occurring after increasing 18βGA incubation times shows a strong correlation (gradient of 0.82 and R^2 value of 0.95; Figure 5D). Since the decrease in outward signal propagation was the same after intervention with either 18βGA (Figure 5B) or a decrease in photolysis light intensity (Figure 5A), this suggests that a major mechanism of action of the reported gap junction blockers is to inhibit IP_3-mediated Ca^{2+} release rather than to block gap junctions in the endothelium.

CBX and 18βGA have each been reported to evoke cell death (Hasan et al., 2016; Lee, Yang, Kim, Jang, Kim & Myung, 2010; Yu et al., 2014). To investigate whether CBX and 18βGA decreased IP_3-evoked Ca^{2+} release by inducing cell death, the reversibility of the drugs was examined. IP_3-evoked Ca^{2+} signalling evoked by cIP_3 or ACh was examined before incubation, after incubation, and after washout (1 hour) of CBX (Figure 6) or 18βGA, (Figure 7). The inhibitory effects of CBX on Ca^{2+} release evoked by photolysis of IP_3 (Figure 6A-C) or by ACh (Figure 6D-F) were reversed following drug washout. In these experiments, average Ca^{2+} $\Delta F/F_0$ responses significantly decreased during CBX and then significantly increased after the drug was washed out for both the cIP_3-evoked (0.67 ± 0.08 $\Delta F/F_0$ vs 0.18 ± 0.03 $\Delta F/F_0$ vs 0.48 ± 0.07 $\Delta F/F_0$; $n = 5$; $p < 0.05$; Figure 6C) and ACh-evoked (0.27 ± 0.05 $\Delta F/F_0$ vs 0.018 ± 0.007 $\Delta F/F_0$ vs 0.50 ± 0.04 $\Delta F/F_0$; $n = 5$; $p < 0.05$; Figure 6F) activations.

Whilst the number of cells activated by cIP_3 was unaltered by CBX (18 ± 2 vs 17 ± 2 vs 18 ± 2 cells; n = 5; p = 0.3; Figure 6C), the number activated by ACh was significantly decreased and reversed on washout (315 ± 25 vs 76 ± 18 vs 332 ± 15 cells; n = 5; p<0.05; Figure 6F). Washout of 18βGA also resulted in a partial recovery of cIP_3- and ACh-evoked Ca^{2+} signalling (Figure 7). Whilst cIP_3-evoked Ca^{2+} responses were significantly decreased by incubation with 18βGA and $\Delta F/F_0$ increased again after washout (0.52 ± 0.09 $\Delta F/F_0$ vs 0.04 ± 0.03 $\Delta F/F_0$ vs 0.24 ± 0.06 $\Delta F/F_0$; n = 5; p <0.05; Figure 7C), the recovery was not significant for ACh-evoked Ca^{2+} responses (0.4 ± 0.2 $\Delta F/F_0$ vs 0.02 ± 0.02 $\Delta F/F_0$ vs 0.6 ± 0.5 $\Delta F/F_0$; n = 5; p = 0.3; Figure 7F). The number of cells was significantly decreased after incubation with 18βGA and increased again after washout for both IP_3-evoked signals (22 ± 1 vs 6 ± 4 vs 22 ± 1 cells; n = 5; p < 0.05; Figure 7C) and ACh-evoked (317 ± 25 vs 54 ± 19 vs 225 ± 62 cells; n = 5; p < 0.05; Figure 7F). The better recovery on washout for CBX is likely due to the increased water solubility of CBX compared to 18βGA. These results suggest that CBX and 18βGA reversibly inhibit IP_3-mediated Ca^{2+} release.

To further test whether CBX and 18βGA caused cell death, we used propidium iodide staining as an assay of cell membrane permeability and apoptosis. Neither CBX nor 18βGA caused an increase in propidium iodide staining (Supplementary Figure 1). Thus, in the present study, CBX and 18βGA did not evoke endothelial cell death, as measured by the reversibility of the IP_3-evoked Ca^{2+} responses and by propidium iodide staining.

CBX and 18βGA have been shown to inhibit small (SK) and intermediated (IK) conductance potassium channels (Behringer, Socha, Polo-Parada & Segal, 2012) which may alter the plasma membrane potential and have consequences for Ca^{2+} store refilling (McCarron, Flynn, Bradley & Muir, 2000). A block of store refilling could explain the effects of CBX and 18βGA on IP_3-evoked Ca^{2+} release. To determine if the inhibitory effects of CBX and 18βGA arose from K^+-channel-dependent changes in membrane potential, IP_3-evoked endothelial Ca^{2+} responses were recorded in the absence and presence of apamin (100 nM, Figure 8), an SK blocker, or TRAM-34 (1 μM, Figure 8), an IK blocker.

As shown in Figure 8A apamin did not alter ACh-evoked Ca^{2+} signals, whilst CBX abolished the response in these same preparations (Figure 8A-B). Again, the effect of CBX was reversible on washout. The mean amplitude of ACh-evoked Ca^{2+} signals (n=5, 0.35±0.06 vs 0.35±0.05 vs 0.04±0.01 vs 0.41±0.03 F/F_0, p<0.05; Figure 8B) and the number of ACh-

responsive cells (*n*=6, 157 ± 6 vs 157 ± 6 vs 68 ± 9 vs 157 ± 7 cells, $p<0.05$; Figure 8B) confirms this.

TRAM-34 also failed to alter ACh-evoked endothelial Ca^{2+} signalling (Figure 8C-D). The mean amplitude of ACh-evoked Ca^{2+} signals (0.5±0.1 $\Delta F/F_0$ vs 0.44±0.09 $\Delta F/F_0$ vs 0.06±0.02 $\Delta F/F_0$ vs 0.50±0.08 $\Delta F/F_0$; n = 7; $p<0.05$; Figure 8D) and number of ACh-responsive cells (*n*=7, 151 ± 7 vs 151 ± 7 vs 83 ± 7 vs 148 ± 8 cells, $p<0.05$; Figure 8D) were unaltered by the K^+ channel blockers but were subsequently inhibited by CBX. Since neither apamin nor TRAM-43 altered IP_3-mediated Ca^{2+} release, it is unlikely that the inhibitory effects of CBX and 18βGA on IP_3-evoked Ca^{2+} release were mediated by K^+ channel inhibition.

CBX and 18βGA have been reported to collapse the mitochondrial membrane potential ($\Delta\Psi_M$)(Salvi, Fiore, Battaglia, Palermo, Armanini & Toninello, 2005; Wang, Wong, Feng & Zhang, 2014). Collapse of $\Delta\Psi_M$ has widespread effects on cell function, including on the regulation of IP_3-evoked Ca^{2+} release (Correa, Lafayette, Pereira, Hirata, Garcez-do-Carmo & Smaili; Csordas et al., 2006; Narayanan, Xi, Pfeffer & Jaggar, 2010; Olson, Chalmers & McCarron, 2010; Rizzuto, Brini, Murgia & Pozzan, 1993; Rizzuto et al., 1998; Sward, Dreja, Lindqvist, Persson & Hellstrand, 2002; Szado et al., 2003; Zhang, Lee, Wilson & McCarron, 2019). To determine if the $\Delta\Psi_M$ was altered by the drugs, mitochondria were visualised using the membrane potential indicator TMRE (120 nM, 5 mins; Figure 9A) and the effects of CBX and 18βGA on $\Delta\Psi_M$ were examined. CBX and 18βGA each evoked a rapid (within 60s) and reversible depolarisation of $\Delta\Psi_M$ (Figure 9B Baseline and Treatment, Supplementary Video 5), evident from the 'smearing' of the punctate mitochondrial fluorescence signal as TMRE moves from the mitochondria into the cytoplasm. Equally striking was the speed at which mitochondria repolarised on washout of the drugs (Fig 9B, Washout). Recovery occurred within 60s of washout.

The concentration of TMRE in mitochondria is governed by Nernstian function of the mitochondrial membrane potential *and* plasma membrane potential. To ensure that the effect of CBX and 18βGA arose from depolarisation of $\Delta\Psi_M$ rather than depolarisation of the plasma membrane potential, the plasma membrane potential was clamped using a High-K^+ PSS and the experiments repeated (Figure 9C). $Ca^{2+}$was omitted from the bathing solution to prevent smooth muscle contraction. In High K^+-PSS, CBX or 18βGA each again rapidly depolarised $\Delta\Psi_M$ (Figure 9C), as revealed by the loss of punctate TMRE staining. Since the

endothelial plasma membrane potential was clamped by the High K^+-PSS, the effect of CBX or 18βGA is on the mitochondria.

Taken together, these data suggest that CBX and 18βGA have pronounced effects on endothelial function by inhibiting IP_3-evoked Ca^{2+} release and depolarising $\Delta\Psi_M$.

Discussion

Ca^{2+} signals in the endothelium propagate regeneratively among cells to provide the long distance communication essential to coordinate normal vascular function (Lee, Wilson, Saunter, Kennedy, Girkin & McCarron, 2018; Longden et al., 2017; McCarron, Lee & Wilson, 2017; Tallini et al., 2007; Wilson, Lee & McCarron, 2016b). Movement of small molecules such as IP_3 or Ca^{2+} through gap junctions is proposed to underlie Ca^{2+} signal propagation and aberrant gap junction function may participate in cardiovascular disease development (Pohl, 2020). In the study of gap junction function, carbenoxolone (CBX) and 18β glycyrrhetinic acid (18βGA) are among the most widely used pharmacological agents. Here we show these drugs do not appear to block gap junctions activity when used at concentrations and incubation times reported to block gap junctions (Behringer, Socha, Polo-Parada & Segal, 2012; Boittin, Alonso, Le Gal, Allagnat, Beny & Haefliger, 2013; Kim et al., 2017; Okamoto, Akita, Kawamoto, Hayashi, Suzuki & Shimaoka, 2014; Spray, Ye & Ransom, 2006). Rather, CBX and 18βGA each inhibit endothelial IP_3R activity and collapse the mitochondrial membrane potential ($\Delta\Psi_M$). These findings cast significant doubt on the usefulness of CBX and 18βGA in studies of gap junction contribution to cell communication.

The mechanisms by which CBX and 18βGA block gap junctions are unclear (reviewed in Willebrords, Maes, Crespo Yanguas & Vinken, 2017). 18βGA-mediated inhibition of Cx43 may occur via dephosphorylation of type 1 or type 2A protein phosphatases (Guan, Wilson, Schlender & Ruch, 1996), and direct interaction with the connexin has also been proposed to occur (Davidson & Baumgarten, 1988). There have been no studies clearly defining the mechanisms behind CBX inhibition of connexin channels (Leybaert et al., 2017). There are several reports of 'off-target' effects which may account for some of the effects of 18βGA and CBX on cell-cell communication. Glycyrrhetinic acids bind strongly to mineralocorticoid and glucocorticoid receptors (Armanini, Karbowiak & Funder, 1983; Kratschmar et al., 2011), inhibit 11β-hydroxysteroid dehydrogenase and act in anti-inflammatory roles through these pathways (Morsy et al., 2019). CBX also shows high affinity for the mineralocorticoid receptor (Armanini, Karbowiak, Krozowski, Funder & Adam, 1982).

In rat small mesenteric arteries, 18βGA (30μM) blocked Ca^{2+} currents in smooth muscle cells (Matchkov, Rahman, Peng, Nilsson & Aalkjaer, 2004). CBX (100μM) also blocked voltage-gated Ca^{2+} currents and reduced Ca^{2+} influx and depolarization-evoked Ca^{2+} signals in Salamander retina (Vessey, Lalonde, Mizan, Welch, Kelly & Barnes, 2004). In cultured

astrocytes, spontaneous action potentials, synaptic currents and synchronised Ca^{2+} oscillations were also inhibited with 100μM CBX, independently of gap junctions (Rouach, Segal, Koulakoff, Giaume & Avignone, 2003). Cl^- currents were blocked by 40μM 18βGA in primary rat hepatocytes (Bohmer, Kirschner & Wehner, 2001), and delayed rectified K^+ currents at concentrations up to 10μM 18βGA in guinea pig myocytes. In endothelial tubes, IK/SK channel-mediated hyperpolarization was blocked by either 18βGA (up to 40μM) or CBX (up to 100μM) (Behringer, Socha, Polo-Parada & Segal, 2012). There are no previous reports of these drugs in the context of IP_3R or IP_3-mediated Ca^{2+} release, though other studies have found a reduction in IP_3-mediated activity upon CBX or 18βGA incubation but attributed the results to gap junction effects. For example, CBX (100 μM) inhibited ACh-mediated Ca^{2+} release in the intact mouse aortic endothelium (Boittin, Alonso, Le Gal, Allagnat, Beny & Haefliger, 2013) and blocked incremental IP_3 increase in the guinea pig cochlea (Gossman & Zhao, 2008).

An alteration in K^+-channel activity (Behringer, Socha, Polo-Parada & Segal, 2012) by CBX and 18βGA could alter the plasma membrane potential and store refilling, providing an explanation for the decreased IP_3-evoked Ca^{2+} release. However, in the present study, there was no effect of either an SK-channel blocker (apamin) or IK-channel blocker (TRAM 34) on IP_3-mediated Ca^{2+} release. This suggests that inhibition of K^+-channel activity is an unlikely explanation of CBX- and 18βGA-mediated inhibition of IP_3-mediated Ca^{2+} release in mesenteric artery endothelium.

Another unexpected finding in the present study was the collapse of the mitochondrial membrane potential ($\Delta\Psi_M$) induced by each of the gap junction blockers. The collapse of $\Delta\Psi_M$ will have wide ranging effects on cell signalling. The CBX- and 18βGA-induced collapse of $\Delta\Psi_M$ (measured with TMRE) occurred in normal PSS and in a high-K^+ PSS that was used to clamp the plasma membrane potential. The concentration of TMRE in mitochondria is a Nernstian function of the $\Delta\Psi_M$ and plasma membrane potential, therefore the finding that the change in TMRE fluorescence persisted in a high-K^+ PSS confirms that CBX and 18βGA alter $\Delta\Psi_M$, not the endothelial plasma membrane potential.

CBX and 18βGA have previously been reported to depolarise $\Delta\Psi_M$. For example, in a pituitary adenoma cell line, 18βGA (up to 150μM) caused a decrease in $\Delta\Psi_M$ and elevated intracellular ROS and Ca^{2+} concentrations, stimulating mitochondrial permeability transition (MMP) leading to increased apoptosis (Wang, Wong, Feng & Zhang, 2014). In ovarian

carcinoma cell lines, 18βGA evoked apoptosis via potentiation of trichostatin A (1-25μM, 24hrs) (Lee, Yang, Kim, Jang, Kim & Myung, 2010) and $\Delta\Psi_M$ depolarisation leading to Hsp90 inhibition-mediated caspase 8 activation (Yang, Myung, Kim & Lee, 2012) or cytochrome c release and caspase-3 activation (Lee, Kim, Lee, Han & Lee, 2008). 18βGA-induced mitochondrial membrane changes and apoptosis occurs in human bladder cancer (Lin, Huang, Hour, Yang, Pu & Lin, 2011), human endometrial stromal (Yu et al., 2014), and human hepatoma cell lines (Hasan et al., 2016). CBX also induced $\Delta\Psi_M$ collapse in liver mitochondria, resulting in mitochondrial permeability transition and apoptosis (Salvi, Fiore, Battaglia, Palermo, Armanini & Toninello, 2005).

While CBX and 18βGA each depolarised $\Delta\Psi_M$, we did not observe endothelial cell apoptosis in the present study at the concentrations and incubation times used, as shown by the lack of propidium iodide-positive staining (Supplementary Figure 1) and the reversibility of the drug effects on Ca^{2+} signalling and $\Delta\Psi_M$ depolarisation. CBX has better water solubility than 18βGA (Leybaert et al., 2017) and therefore the washout of CBX was more effective than that of 18βGA. Notwithstanding, we did observe that leaving the drug on longer than the ~10 mins for CBX or ~1hr for 18βGA caused a significant, irreversible increase in resting Ca^{2+} concentration in some cells (data not shown).

Collapse of $\Delta\Psi_M$ by CBX and 18βGA could explain the changes in IP_3-evoked Ca^{2+} release (Correa, Lafayette, Pereira, Hirata, Garcez-do-Carmo & Smaili; Csordas et al., 2006; Narayanan, Xi, Pfeffer & Jaggar, 2010; Olson, Chalmers & McCarron, 2010; Rizzuto, Brini, Murgia & Pozzan, 1993; Rizzuto et al., 1998; Sward, Dreja, Lindqvist, Persson & Hellstrand, 2002; Szado et al., 2003; Zhang, Lee, Wilson & McCarron, 2019). For example, in the endothelium, reactive oxygen species such as hydrogen peroxide depolarize $\Delta\Psi_M$ leading to inhibition of IP_3-evoked Ca^{2+} release (Zhang, Lee, Wilson & McCarron, 2019). The uncoupler carbonyl cyanide 3-chlorophenylhydrazone (CCCP) or complex 1 inhibitor, rotenone also inhibited IP_3-evoked Ca^{2+} release in the endothelium by $\Delta\Psi_M$ depolarisation (Zhang, Lee, Wilson & McCarron, 2019). Our results therefore raised the possibility that CBX and 18βGA inhibit IP_3-mediated Ca^{2+} release by $\Delta\Psi_M$ depolarisation. However, depolarisation of $\Delta\Psi_M$ by CBX or 18βGA occurred rapidly (within 90 s) while inhibition of IP_3-mediated Ca^{2+} release developed more slowly (5 mins for CBX; 45 mins for 18βGA). The differences in time course suggests that $\Delta\Psi_M$ depolarisation alone does not explain the inhibition of IP_3-evoked Ca^{2+} release and that CBX or 18βGA block IP_3R.

Together, our study questions the usefulness of CBX and 18βGA in gap junction studies in intact tissue. CBX and 18βGA each inhibit IP_3-mediated Ca^{2+} release and depolarise $\Delta\Psi_M$ but do not appear to block cell communication via gap junctions.

Author contributions:
CB CW & JGM developed the concept. CB & XZ performed the experiments. CB, XZ, CW analysed the data. CB, XZ, CW & JGM interpreted the data. CB & JGM drafted the manuscript. CB CW XZ & JGM edited the manuscript. CW, CB & JGM sourced funding. All authors approved the final version of the manuscript.

Acknowledgments

This work was funded by the Wellcome Trust (202924/Z/16/Z; 204682/Z/16/Z) and the British Heart Foundation (PG/16/54/32230; PG16/82/32439, PG/20/9/34859), whose support is gratefully acknowledged. The authors would like to thank Margaret MacDonald for her excellent technical support.

Competing Interests

None

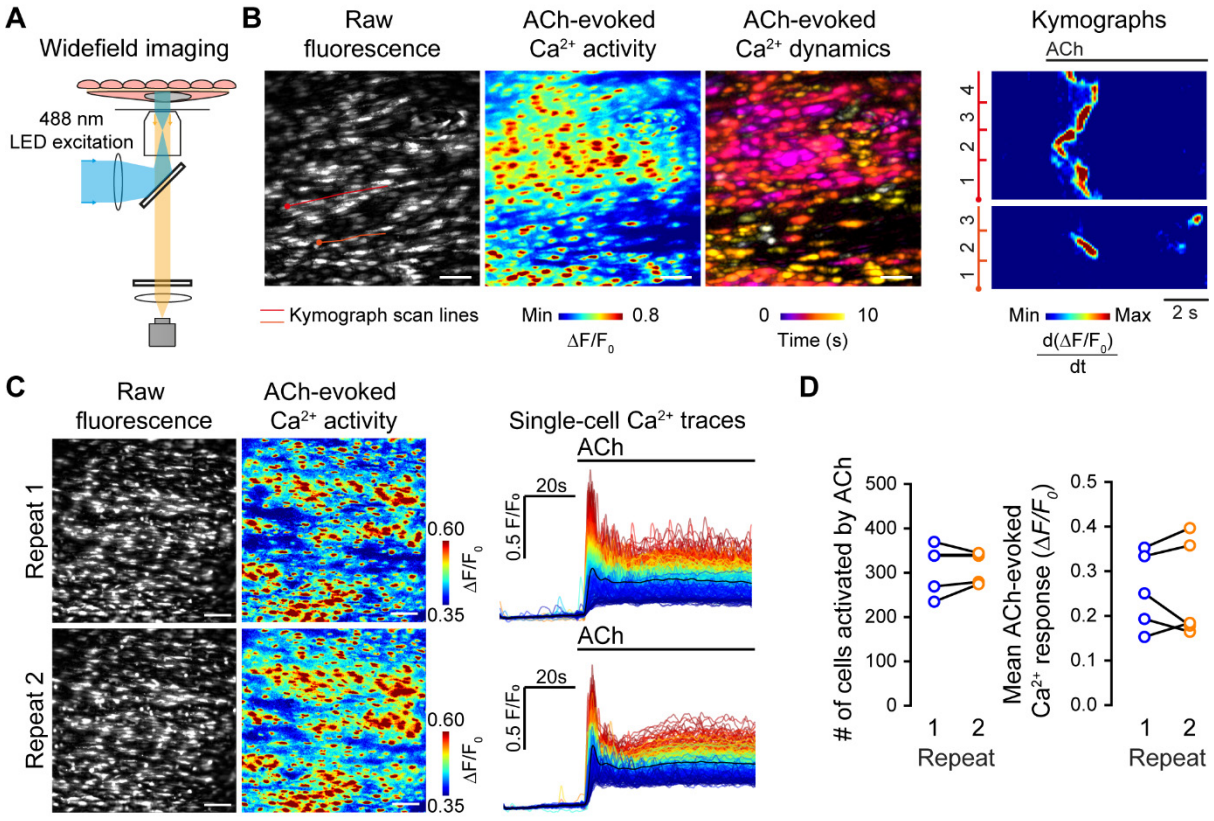

Figure 1: ACh-evoked Ca^{2+} increases are reproducible. (A) Schematic of widefield microscopy for endothelial cell imaging of intact arteries. (B) Representative Ca^{2+} images and kymograph illustrating temporal dynamics of ACh (50 nM)-evoked endothelial Ca^{2+} activity. Ca^{2+} images show raw fluorescence (left), $\Delta F/F_0$ maximum intensity projection (middle), and temporally color-coded projection of active Ca^{2+} wave fronts (determined by sequential subtraction). The kymographs show changes in Ca^{2+} levels across scanlines spanning 4 (red) or 3 (orange) cells. (C) Example raw and pseudocoloured Ca^{2+} images and corresponding single-cell Ca^{2+} traces (black line average) illustrating the response of a single field of endothelial cells to repeat application of ACh (50 nM, 30-minute equilibration between recordings). (D) Summary data illustrating changes in the number of cells activated by successive ACh application (left) and the mean amplitude of the Ca^{2+} response (n = 5). * indicates statistical significance ($p < 0.05$) using paired t-test. All image scale bars = 50 µm.

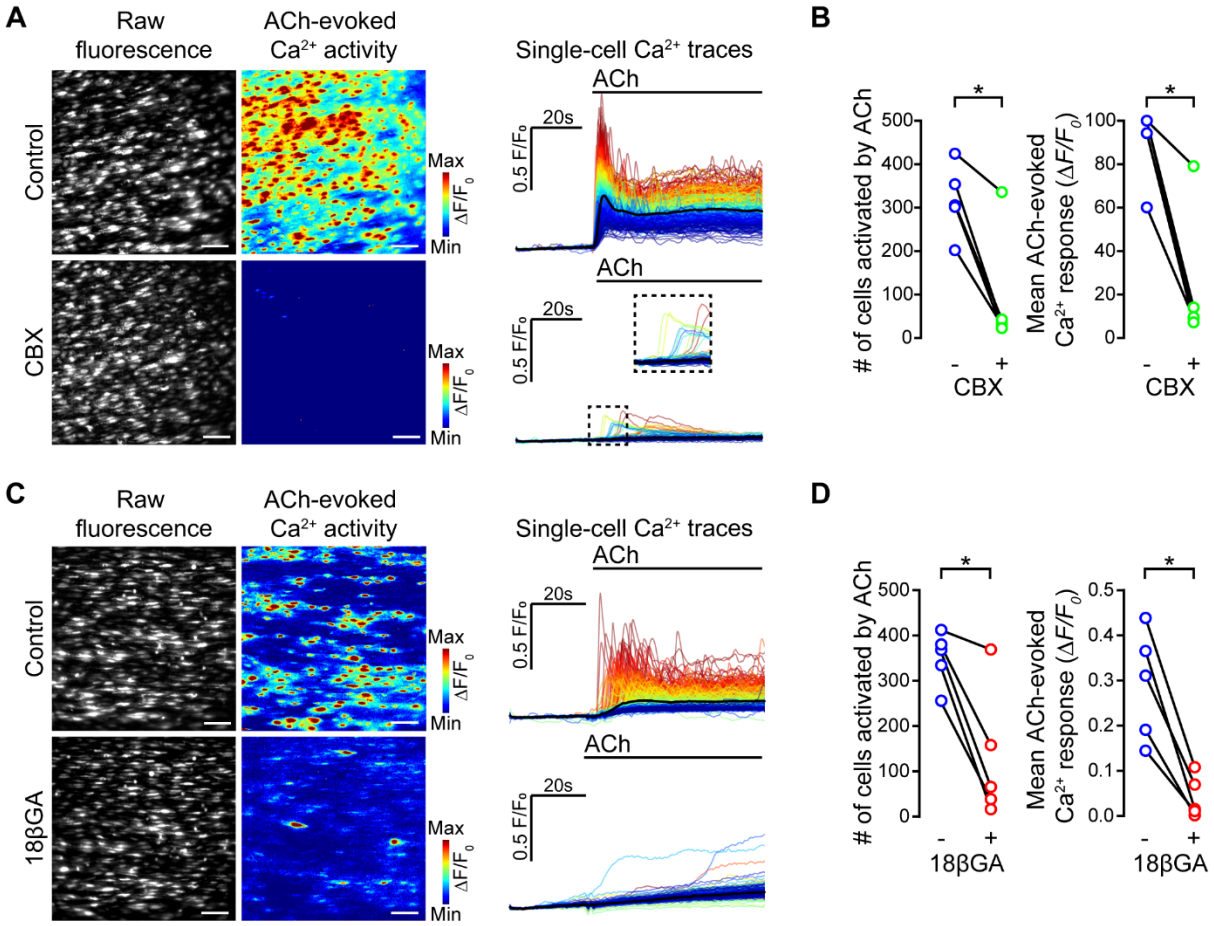

Figure 2: Putative gap junction blockers inhibit ACh-evoked endothelial Ca^{2+} responses. (A-D) Effect of carbenoxolone CBX (A-B; 100 µM, 5 min incubation) and 18βGA (C-D; 40 µM, 45 min incubation) on ACh-evoked (50nM) endothelial cell Ca^{2+} signalling. Panels show: A&C, raw baseline Ca^{2+} images, ACh-evoked Ca^{2+} activity images (pseudocoloured max $\Delta F/F_0$), and corresponding single-cell Ca^{2+} traces (black line average) obtained from the same field of endothelial cells before and after incubation with the indicated inhibitor; B&D, paired summary data plots showing the effect of the indicated inhibitor on the number of cells activated by ACh (left) and the mean amplitude of the ACh-evoked Ca^{2+} response. * indicates statistical significance ($p < 0.05$) using paired t-test. All image scale bars = 50 µm.

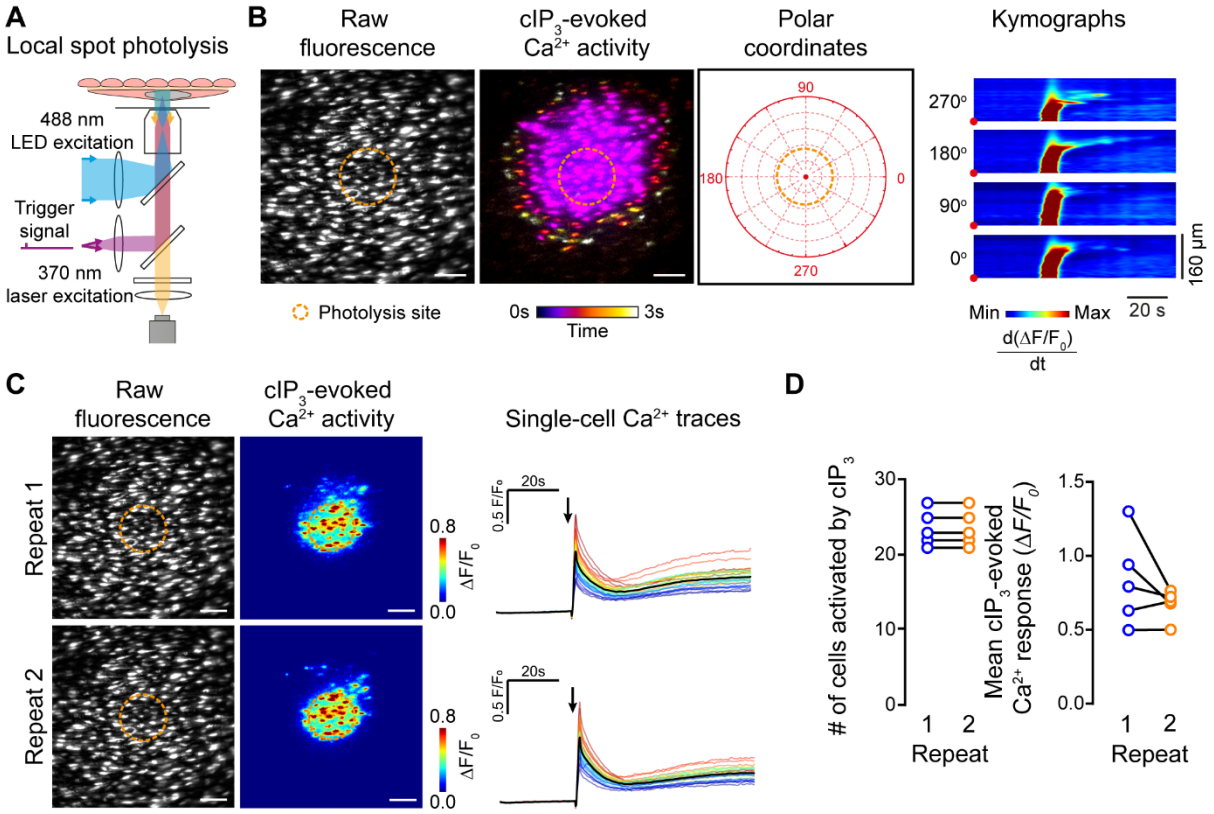

Figure 3: cIP$_3$-evoked increases in endothelial Ca^{2+} levels are reproducible.(A) Schematic of localised photolysis of cIP$_3$ with simultaneous widefield endothelial cell imaging of intact arteries. (B) Representative Ca^{2+} images and kymograph illustrating temporal dynamics of cIP$_3$-evoked endothelial Ca^{2+} activity. Ca^{2+} images show raw fluorescence (left), temporally color-coded projection of active Ca^{2+} wave fronts (determined by sequential subtraction, middle; photolysis region shown by dotted line), and the polar coordinates used for the kymograph. (C) Example raw and pseudocoloured Ca^{2+} images and corresponding single-cell Ca^{2+} traces (black line average) illustrating the response of a single field of endothelial cells to repeat photolysis of cIP$_3$ (30-minute equilibration between recordings). (D) Summary data illustrating the number of cells activated by successive ACh application (left) and the mean amplitude of the Ca^{2+} response (n = 5). Arrow indicates uncaging event. * indicates statistical significance ($p < 0.05$) using paired t-test. All image scale bars = 50 µm.

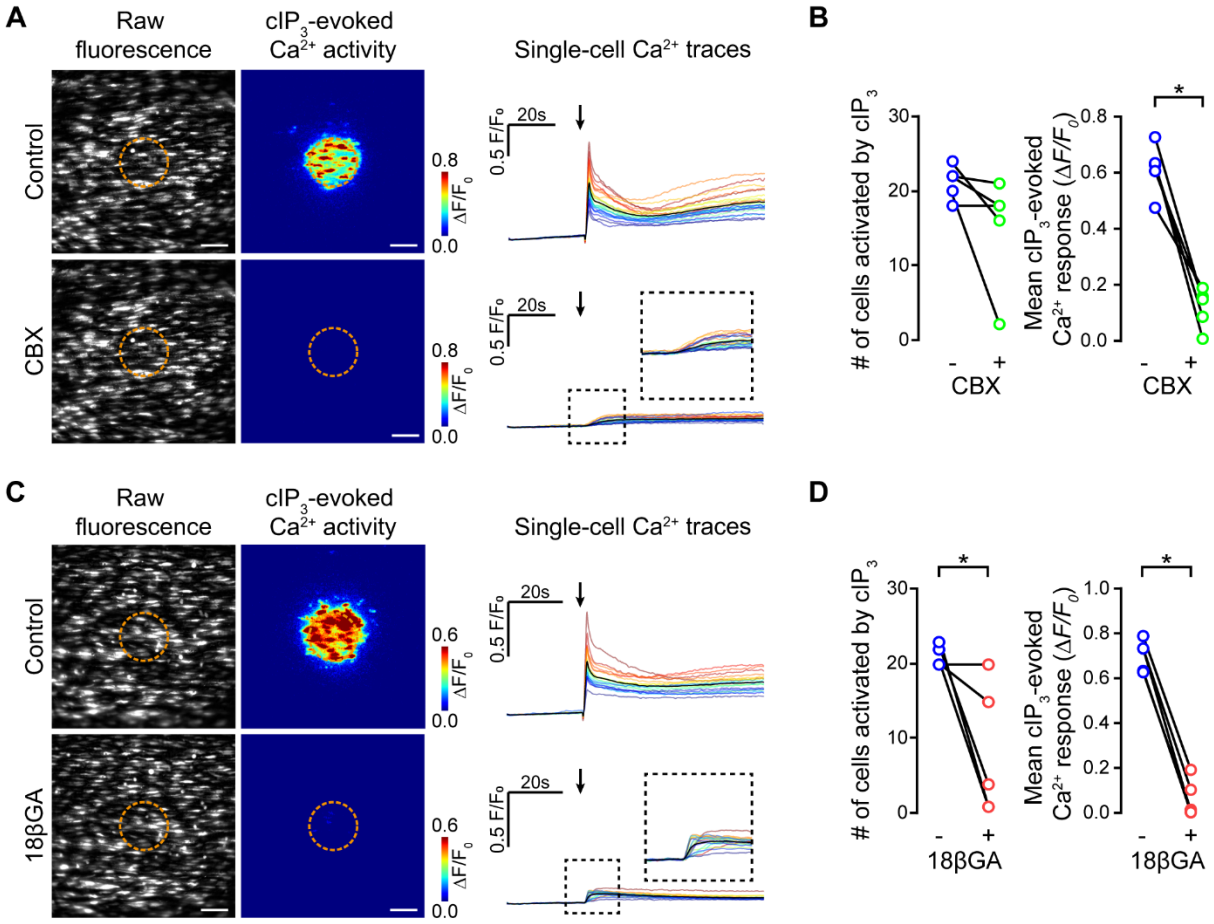

Figure 4: Putative gap junction blockers inhibit cIP$_3$-evoked endothelial Ca^{2+} responses. (A-D) Effect of carbenoxolone CBX (A-B; 100 µM, 5 min incubation) and 18βGA (C-D; 40 µM, 45 min incubation) on cIP$_3$-evoked (5µM) endothelial cell Ca^{2+} signalling. Panels show: A&C, raw baseline Ca^{2+} images, cIP$_3$-evoked Ca^{2+} activity images (pseudocoloured max $\Delta F/F_0$; dotted line shows photolysis site), and corresponding single-cell Ca^{2+} traces (black line average) obtained from the same field of endothelial cells before and after incubation with the indicated inhibitor. Arrow indicates uncaging event. B&D, paired summary data plots showing the effect of the indicated inhibitor on the number of cells activated by cIP$_3$ (left) and the mean amplitude of the cIP$_3$-evoked Ca^{2+} response (right). * indicates statistical significance ($p < 0.05$) using paired t-test. All image scale bars = 50 µm.

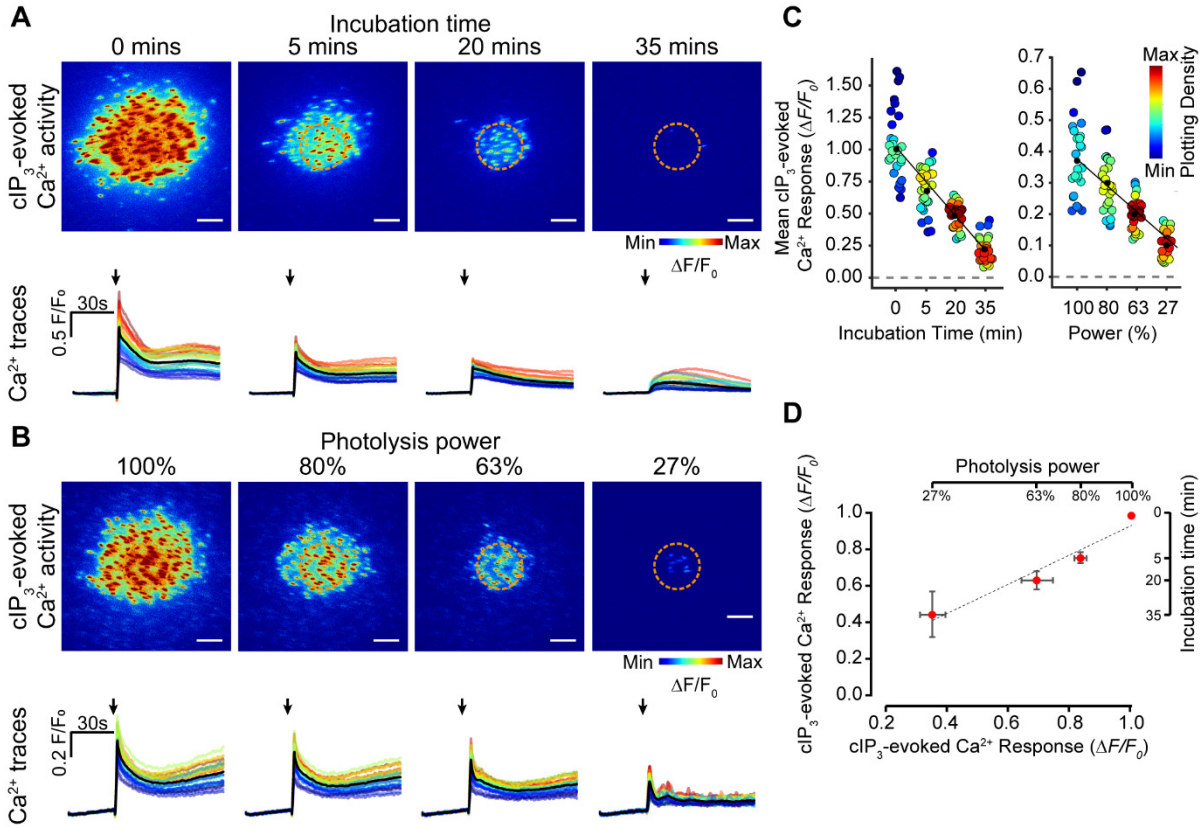

Figure 5: 18βGA suppresses cell-cell communication by decreasing IP_3-evoked Ca^{2+} release. (A) Effect of 18βGA (40 µM) incubation for 5 mins, 20 mins or 35 mins on cIP_3-evoked endothelial cell Ca^{2+} signalling. (B) Effect of decreasing photolysis power on cIP_3-evoked endothelial cell Ca^{2+} signalling. Panels show cIP_3-evoked Ca^{2+} activity images (pseudocoloured max $\Delta F/F_0$ over 2s post uncaging), and corresponding single-cell Ca^{2+} traces (black line average) obtained from the same field of endothelial cells under the indicated condition. Arrows indicate uncaging event. (C) Mean cIP_3-evoked Ca^{2+} response from each cell shown in A) (left) or B (right). Points are colour coordinated according to plotting density (blue low, red high), and a line of best fit plotted. (D) Scatterplot showing the relationship between cIP_3-evoked responses elicited at different stimulation intensities and those evoked after various18βGA incubation times. Grey line shows the linear line of best fit (n=5, error bars: SEM). Scale bars = 50 µm.

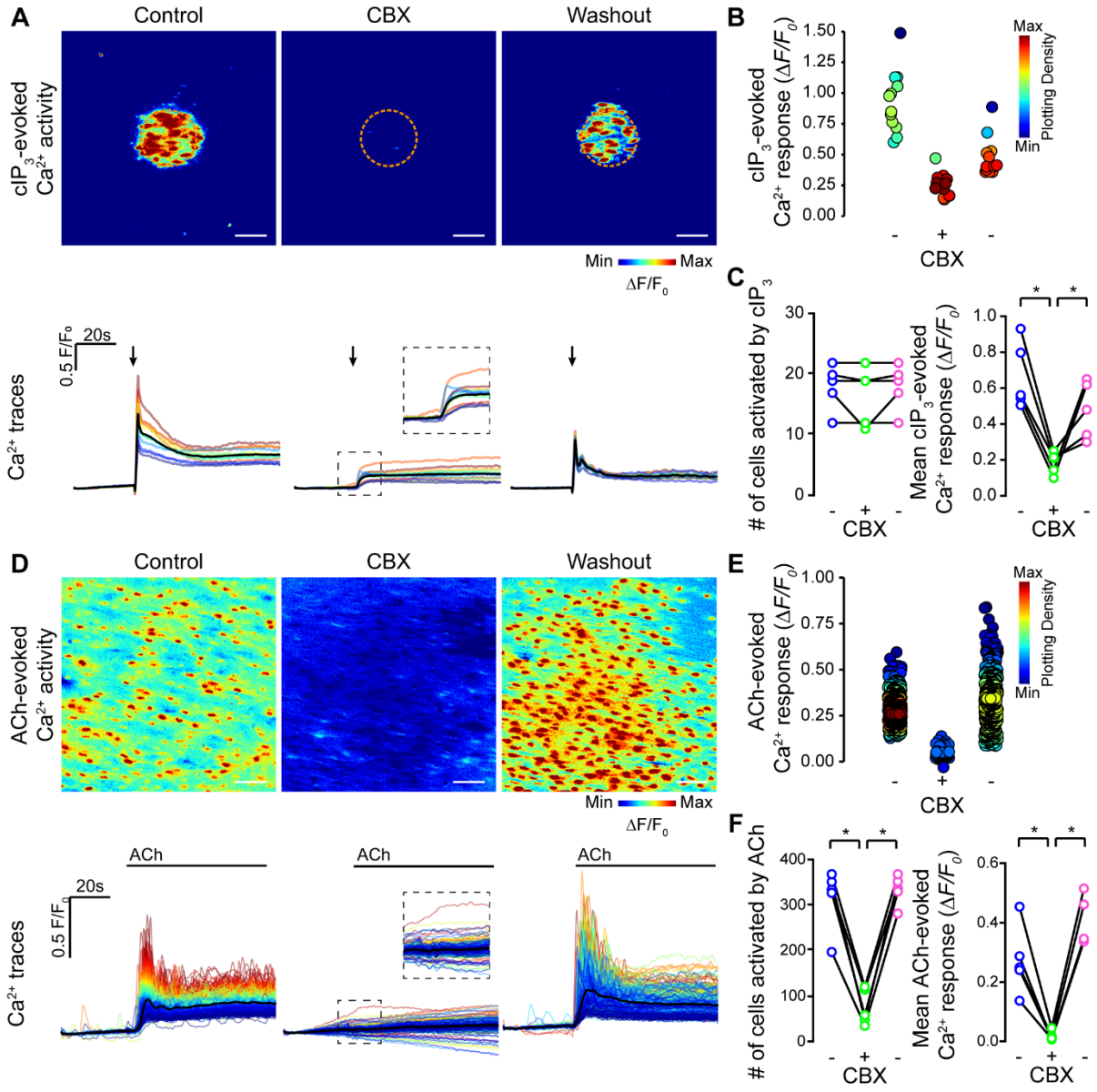

Figure 6: Inhibition of IP_3-mediated Ca^{2+} release by CBX is reversible. Effect of CBX incubation (100 µM, 5 min incubation) and washout (1hr, PSS) on (A-C) cIP_3-evoked (5µM) and ACh-evoked (D-F) endothelial cell Ca^{2+} signalling. Panels show: A&D, cIP_3-evoked Ca^{2+} activity images (pseudocoloured max $\Delta F/F_0$), and corresponding single-cell Ca^{2+} traces (black line average) obtained from the same field of endothelial cells before and after incubation with, and after washout of, CBX. Arrows indicate uncaging event. B&E, mean Ca^{2+} response from each cell in the endothelial field shown under each condition. Points are colour coordinated according to plotting density; C&F, paired summary data plots showing the effect of CBX incubation and washout on the number of cells activated by cIP_3 (left) and the mean amplitude of the Ca^{2+} response. * indicates statistical significance ($p < 0.05$) using paired one-way ANOVA with Tukey's multiple comparisons test; n = 5. All image scale bars = 50 µm.

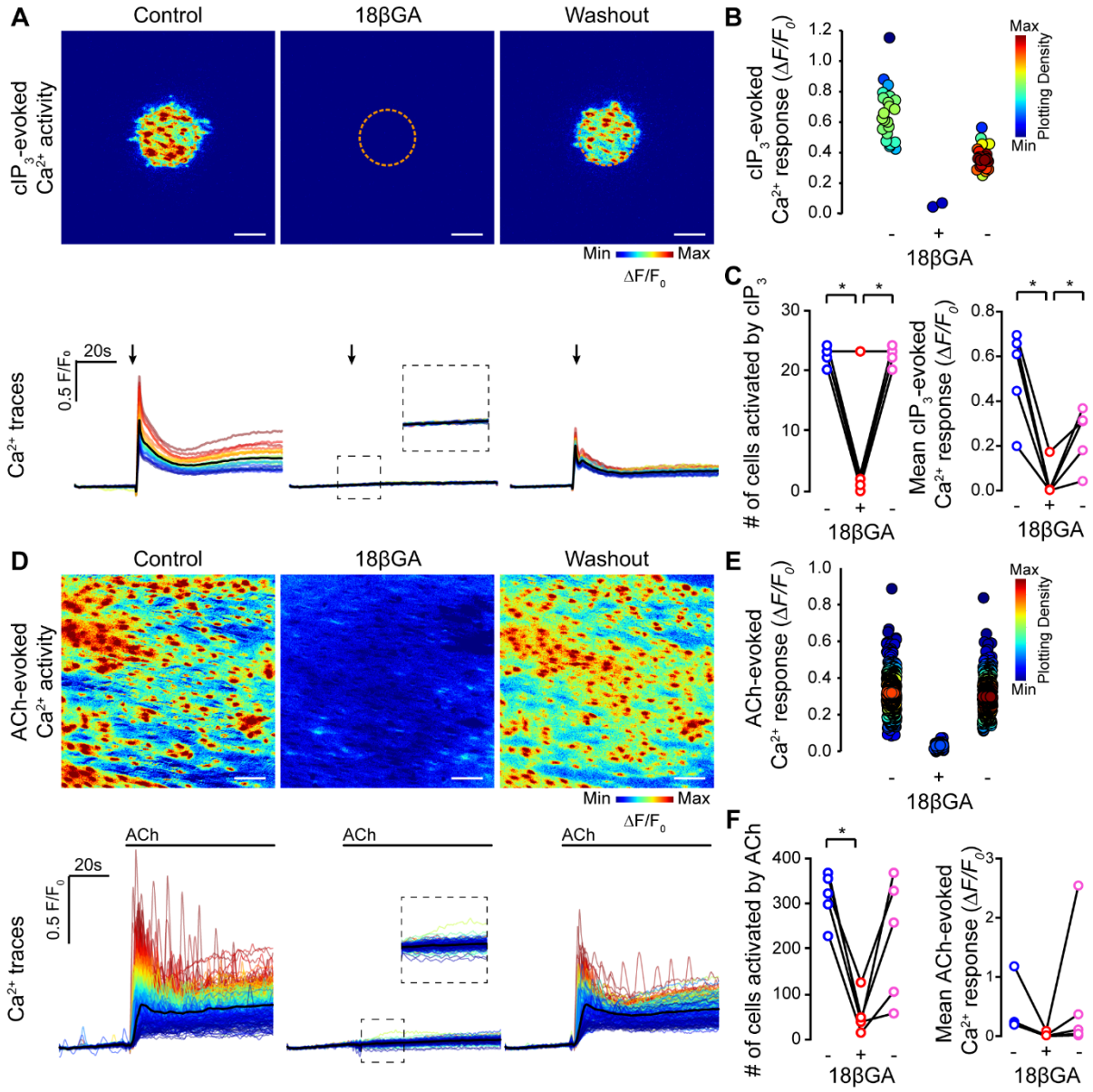

Figure 7: Inhibition of IP_3-mediated Ca^{2+} release by 18βGA is partially reversible
Effect of 18βGA incubation (40 µM, 45 min incubation) and washout (1hr, PSS) on (A-C) cIP_3-evoked (5µM) and ACh-evoked (D-F) endothelial cell Ca^{2+} signalling. Panels show: A&D, cIP_3-evoked Ca^{2+} activity images (pseudocoloured max $\Delta F/F_0$), and corresponding single-cell Ca^{2+} traces (black line average) obtained from the same field of endothelial cells before and after incubation with, and after washout of, 18βGA. Arrows indicate uncaging event. B&E, mean Ca^{2+} response from each cell in the endothelial field shown under each condition. Points are colour coordinated according to plotting density; C&F, paired summary data plots showing the effect of 18βGA incubation and washout on the number of cells activated by cIP_3 (left) and the mean amplitude of the Ca^{2+} response. * indicates statistical significance ($p < 0.05$) using paired one way ANOVA with Tukey's multiple comparisons test; n = 5. All image scale bars = 50 µm.

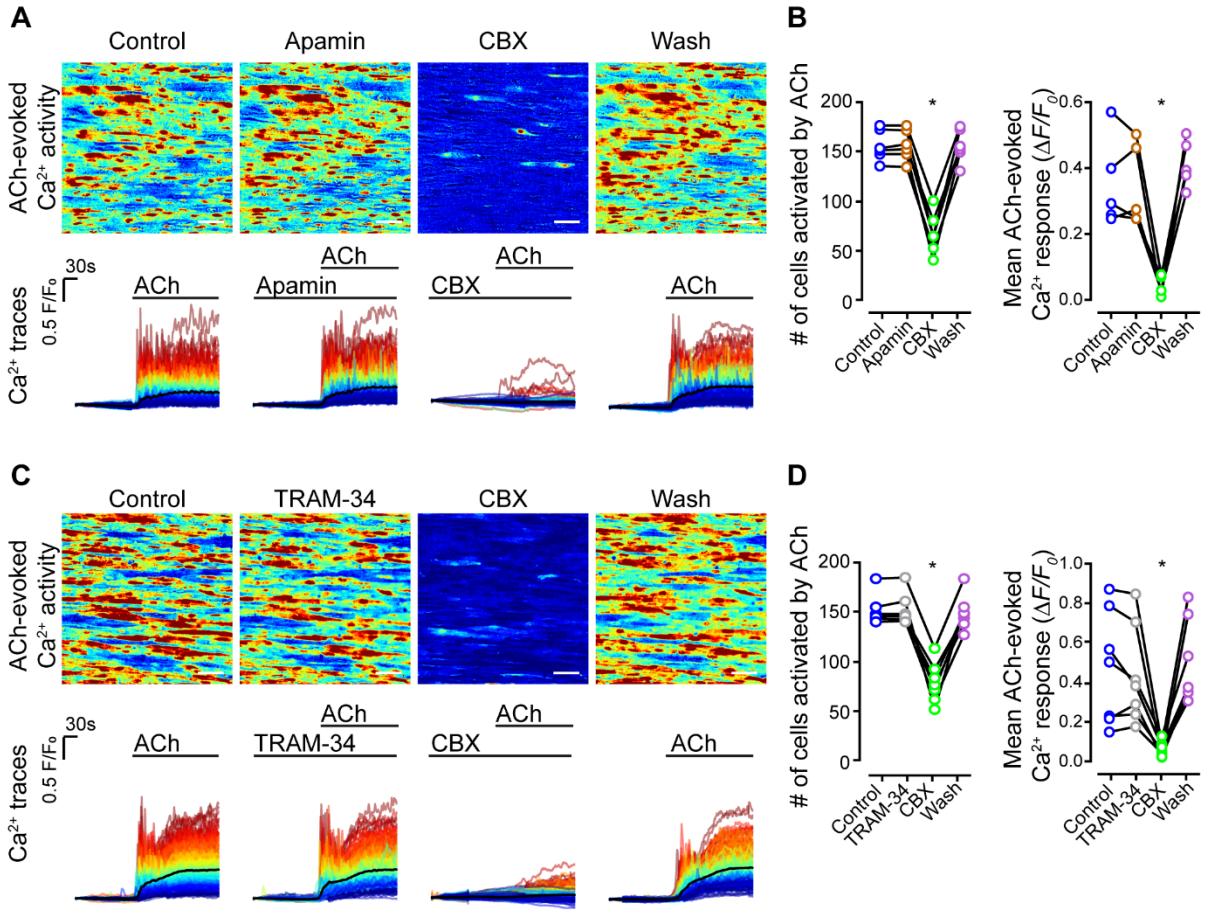

Figure 8: CBX inhibitory action is not due to blockade of small or intermediate conductance K^+ channels. Effect of (A-B) small (Apamin, 100 nM, 10 mins incubation) and (C-D) intermediate conductance (TRAM-34, 1 µM, 10 mins incubation) K^+-channel block on ACh-evoked (100 nM) endothelial cell Ca^{2+} signalling. Panels show: A&C, ACh-evoked Ca^{2+} activity images (pseudocoloured max $\Delta F/F_0$), and corresponding single-cell Ca^{2+} traces (black line average) obtained from the same field of endothelial cells for a control recording, after incubation with TRAM-34, after incubation with CBX, and after washout of all drugs; B&D, paired summary data plots showing the effect of incubation of the indicated drug and washout on the number of cells activated by ACh (left) and the mean amplitude of the Ca^{2+} response. * indicates statistical significance ($p < 0.05$) using paired one way ANOVA with Tukey's multiple comparisons test; n = 5. All image scale bars = 50 µm.

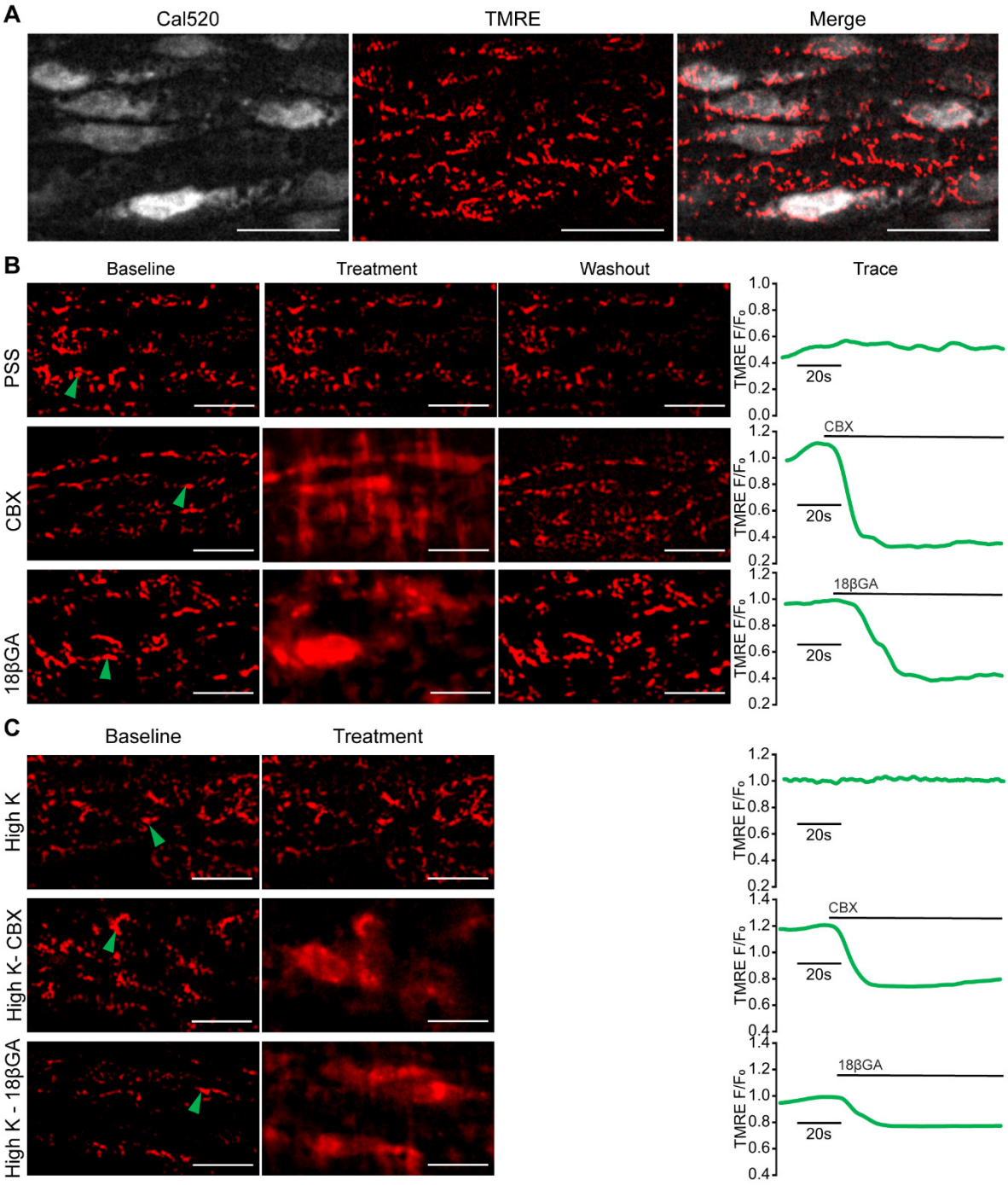

Figure 9: CBX and 18βGA each rapidly depolarise the mitochondrial membrane potential (A) Endothelial cells from *en face* mesenteric artery preparations were stained with Cal-520 (5 μM, green) and TMRE (150 nM, red) to visualise the mitochondrial membrane potential ($\Delta\Psi_M$). (B) Mitochondria were imaged for 1.5 mins whilst administering PSS (control), CBX (100 μM) or 18βGA (40 μM) at 1.5 ml.min^{-1} under constant flow. Fluorescence intensity traces from individual mitochondria (designated by green arrows in the baseline image) are shown from across the treatment period for PSS, CBX and 18βGA administration, indicated with by a bar over the trace. (C) Experiments were repeated in Ca^{2+}-free, High K^+ PSS (control), CBX in Ca^{2+}-free, High K^+ PSS and 18βGA in Ca^{2+}-free, High K^+ PSS, and fluorescence intensity traces from individual mitochondria again shown. Examples from single replicates are shown from n = 5 biological replicates yielding similar results. Scale bars = 25 μm.

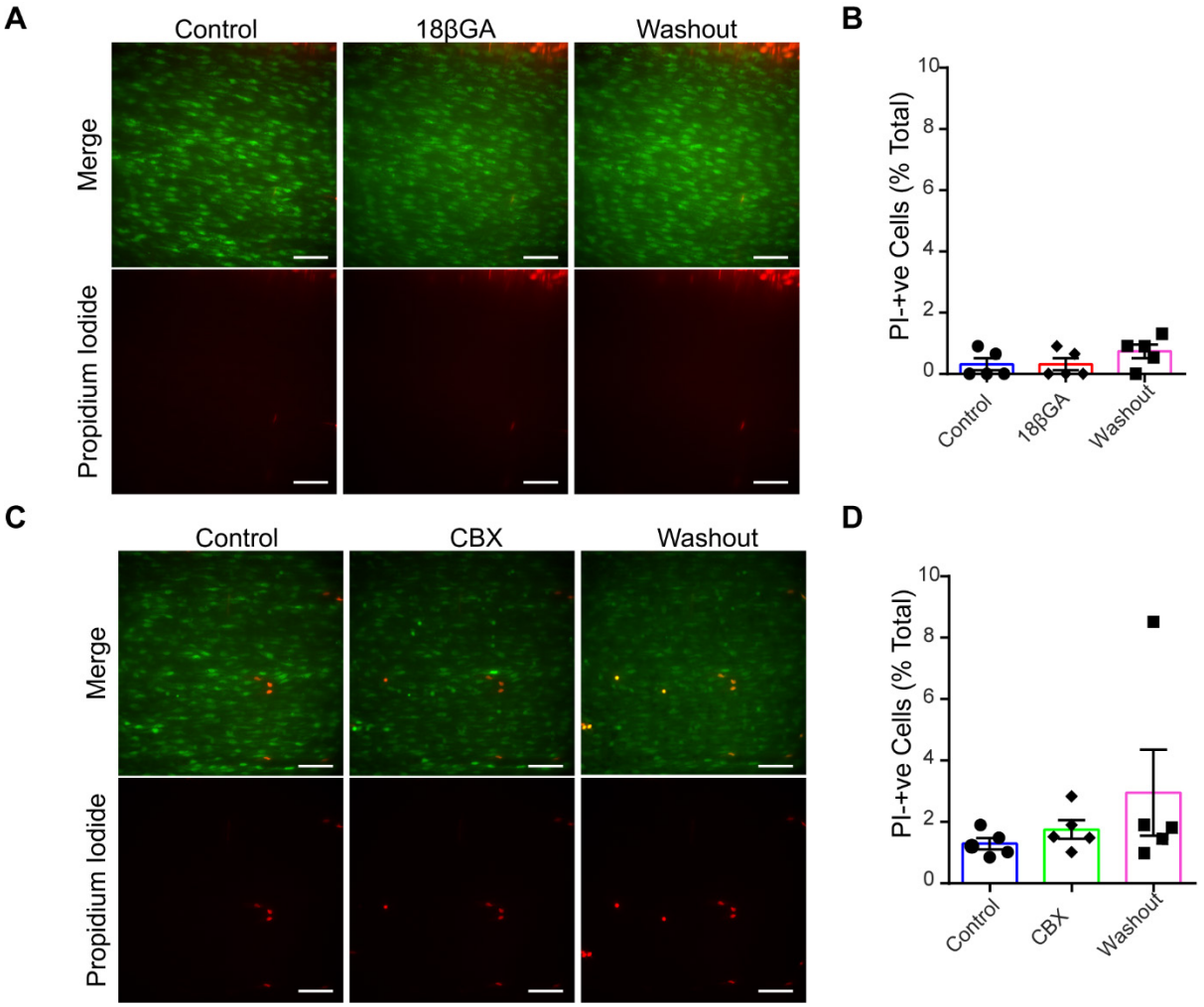

Supplementary Figure 1: Incubation with 18βGA and CBX does not increase membrane permeability

(A,C) E*n face* mesenteric artery preparations were stained with Cal-520 (5 µM, green) and propidium iodide (1.5 µM, red) and control recordings, recordings after incubation with (A) 18βGA (40 µM, 45 mins) or (C) CBX (100 µM, 5 mins), and after 1 hr washout (PSS, 1.5 ml.min^{-1}). (B,D) The number of propidium iodide-positive cells for each condition, plotted as a percentage of the total number of cells in the FoV. Examples from single replicates are shown from n = 5 paired biological replicates. Scale bars = 50 µm.

Supplementary Videos

Supplementary Video 1: ACh evokes reproducible endothelial Ca^{2+} increases
E*n face* mesenteric artery preparation stained with Cal-520 (5 μM, grey) was stimulated with ACh (50nM) after 30s baseline recording (10Hz). The resulting Ca^{2+} activity is visualised in green. Upper image: repeat 1; lower image: repeat 2, taken 30 mins after repeat 1. Scale bars = 50 μm.

Supplementary Video 2: cIP_3 evokes reproducible endothelial Ca^{2+} increases
E*n face* mesenteric artery preparation stained with Cal-520 (5 μM, grey) and cIP_3 (5 μM). Ca^{2+} activity was stimulated by localised photolysis (yellow circle) after 30s baseline recording (10Hz). The resulting Ca^{2+} activity is visualised in green. Upper image: repeat 1; lower image: repeat 2, taken 30 mins after repeat 1 in the same preparation. Scale bars = 50 μm.

Supplementary Video 3: CBX inhibits cIP_3-evoked endothelial Ca^{2+} responses
E*n face* mesenteric artery preparation stained with Cal-520 (5 μM, grey) and cIP_3 (5 μM). Ca^{2+} activity was stimulated by localised photolysis (yellow circle) after 30s baseline recording (10Hz). The resulting Ca^{2+} activity is visualised in green. A control recording was taken (upper image) after which the preparation was left to rest for 15 mins, then incubated in CBX (100 μM) for 5 mins. A second recording was then taken (lower panel). Scale bars = 50 μm.

Supplementary Video 4: 18βGA inhibits cIP_3-evoked endothelial Ca^{2+} responses
E*n face* mesenteric artery preparation stained with Cal-520 (5 μM, grey) and cIP_3 (5 μM). Ca^{2+} activity was stimulated by localised photolysis (yellow circle) after 30s baseline recording (10Hz). The resulting Ca^{2+} activity is visualised in green. A control recording was taken (upper image) after which the preparation was left to rest for 15 mins, then incubated in 18βGA (40 μM) for 45 mins. A second recording was then taken (lower panel). Scale bars = 50 μm.

Supplementary Video 5: CBX rapidly depolarises the mitochondrial membrane potential
E*n face* mesenteric artery preparation were stained with TMRE (150 nM, grey) to visualise the mitochondrial membrane potential ($\Delta\Psi_M$). Mitochondria were imaged for 1.5 mins whilst administering PSS only (upper panel) or PSS+CBX (100 μM) after a baseline recording of 30s at 1.5 $ml.min^{-1}$ under constant flow. Scale bars = 25 μm.

REFERENCES

Armanini D, Karbowiak I, & Funder JW (1983). Affinity of liquorice derivatives for mineralocorticoid and glucocorticoid receptors. Clin Endocrinol (Oxf) 19**:** 609-612.

Armanini D, Karbowiak I, Krozowski Z, Funder JW, & Adam WR (1982). The mechanism of mineralocorticoid action of carbenoxolone. Endocrinology 111**:** 1683-1686.

Bagher P, Beleznai T, Kansui Y, Mitchell R, Garland CJ, & Dora KA (2012). Low intravascular pressure activates endothelial cell TRPV4 channels, local Ca^{2+} events, and IKCa channels, reducing arteriolar tone. Proc Natl Acad Sci U S A 109**:** 18174-18179.

Bagher P, & Segal SS (2011). Regulation of blood flow in the microcirculation: role of conducted vasodilation. Acta Physiol 202**:** 271-284.

Bai D, Yue B, & Aoyama H (2018). Crucial motifs and residues in the extracellular loops influence the formation and specificity of connexin docking. Biochim Biophys Acta Biomembr 1860**:** 9-21.

Behringer EJ, & Segal SS (2012). Tuning electrical conduction along endothelial tubes of resistance arteries through Ca^{2+}-activated K^{+} channels. Circ Res 110**:** 1311-1321.

Behringer EJ, Socha MJ, Polo-Parada L, & Segal SS (2012). Electrical conduction along endothelial cell tubes from mouse feed arteries: confounding actions of glycyrrhetinic acid derivatives. Br J Pharmacol 166**:** 774-787.

Billaud M, Lohman AW, Johnstone SR, Biwer LA, Mutchler S, & Isakson BE (2014). Regulation of cellular communication by signaling microdomains in the blood vessel wall. Pharmacological reviews 66**:** 513-569.

Billaud M, Marthan R, Savineau JP, & Guibert C (2009). Vascular smooth muscle modulates endothelial control of vasoreactivity via reactive oxygen species production through myoendothelial communications. PLoS One 4**:** e6432.

Bodendiek SB, & Raman G (2010). Connexin modulators and their potential targets under the magnifying glass. Curr Med Chem 17**:** 4191-4230.

Bohmer C, Kirschner U, & Wehner F (2001). 18-beta-Glycyrrhetinic acid (BGA) as an electrical uncoupler for intracellular recordings in confluent monolayer cultures. Pflugers Arch 442**:** 688-692.

Boittin FX, Alonso F, Le Gal L, Allagnat F, Beny JL, & Haefliger JA (2013). Connexins and M3 muscarinic receptors contribute to heterogeneous Ca(2+) signaling in mouse aortic endothelium. Cell Physiol Biochem 31**:** 166-178.

Bruzzone R, Barbe MT, Jakob NJ, & Monyer H (2005). Pharmacological properties of homomeric and heteromeric pannexin hemichannels expressed in Xenopus oocytes. J Neurochem 92**:** 1033-1043.

Buckley C, Wilson C, & McCarron JG (2019). FK506 Regulates IP_3-evoked Ca^{2+} release independently of FKBP in Endothelial cells. Br J Pharmacol.

Buckley C, Wilson C, & McCarron JG (2020). FK506 Regulates IP_3-evoked Ca^{2+} release independently of FKBP in Endothelial cells. Br J Pharmacol 177**:** 1131–1149.

Correa RM, Lafayette SS, Pereira GJ, Hirata H, Garcez-do-Carmo L, & Smaili SS Mitochondrial involvement in carbachol-induced intracellular Ca^{2+} mobilization and contraction in rat gastric smooth muscle. Life Sci 89**:** 757-764.

Csordas G, Renken C, Varnai P, Walter L, Weaver D, Buttle KF*, et al.* (2006). Structural and functional features and significance of the physical linkage between ER and mitochondria. J Cell Biol 174**:** 915-921.

Davidson JS, & Baumgarten IM (1988). Glycyrrhetinic acid derivatives: a novel class of inhibitors of gap-junctional intercellular communication. Structure-activity relationships. J Pharmacol Exp Ther 246**:** 1104-1107.

Edelstein AD, Tsuchida MA, Amodaj N, Pinkard H, Vale RD, & Stuurman N (2014). Advanced methods of microscope control using muManager software. Journal of biological methods 1.

Emerson GG, & Segal SS (2000a). Electrical coupling between endothelial cells and smooth muscle cells in hamster feed arteries: role in vasomotor control. Circ Res 87**:** 474-479.

Emerson GG, & Segal SS (2000b). Endothelial cell pathway for conduction of hyperpolarization and vasodilation along hamster feed artery. Circ Res 86**:** 94-100.

Goldberg GS, Moreno AP, & Lampe PD (2002). Gap junctions between cells expressing connexin 43 or 32 show inverse permselectivity to adenosine and ATP. J Biol Chem 277**:** 36725-36730.

Gossman DG, & Zhao HB (2008). Hemichannel-mediated inositol 1,4,5-trisphosphate (IP3) release in the cochlea: a novel mechanism of IP3 intercellular signaling. Cell Commun Adhes 15**:** 305-315.

Guan X, Wilson S, Schlender KK, & Ruch RJ (1996). Gap-junction disassembly and connexin 43 dephosphorylation induced by 18 beta-glycyrrhetinic acid. Mol Carcinog 16**:** 157-164.

Hasan SK, Siddiqi A, Nafees S, Ali N, Rashid S, Ali R*, et al.* (2016). Chemopreventive effect of 18beta-glycyrrhetinic acid via modulation of inflammatory markers and induction of apoptosis in human hepatoma cell line (HepG2). Mol Cell Biochem 416**:** 169-177.

Hernandez VH, Bortolozzi M, Pertegato V, Beltramello M, Giarin M, Zaccolo M*, et al.* (2007). Unitary permeability of gap junction channels to second messengers measured by FRET microscopy. Nat Methods 4**:** 353-358.

Kameritsch P, Pogoda K, Ritter A, Munzing S, & Pohl U (2012). Gap junctional communication controls the overall endothelial calcium response to vasoactive agonists. Cardiovasc Res 93**:** 508-515.

Kim Y, Griffin JM, Harris PW, Chan SH, Nicholson LF, Brimble MA*, et al.* (2017). Characterizing the mode of action of extracellular Connexin43 channel blocking mimetic peptides in an in vitro ischemia injury model. Biochim Biophys Acta Gen Subj 1861**:** 68-78.

Kratschmar DV, Vuorinen A, Da Cunha T, Wolber G, Classen-Houben D, Doblhoff O*, et al.* (2011). Characterization of activity and binding mode of glycyrrhetinic acid derivatives inhibiting 11beta-hydroxysteroid dehydrogenase type 2. J Steroid Biochem Mol Biol 125**:** 129-142.

Ledoux J, Taylor MS, Bonev AD, Hannah RM, Solodushko V, Shui B*, et al.* (2008). Functional architecture of inositol 1,4,5-trisphosphate signaling in restricted spaces of myoendothelial projections. Proc Natl Acad Sci U S A 105**:** 9627-9632.

Lee CS, Kim YJ, Lee MS, Han ES, & Lee SJ (2008). 18beta-Glycyrrhetinic acid induces apoptotic cell death in SiHa cells and exhibits a synergistic effect against antibiotic anti-cancer drug toxicity. Life Sci 83**:** 481-489.

Lee CS, Yang JC, Kim YJ, Jang ER, Kim W, & Myung SC (2010). 18beta-Glycyrrhetinic acid potentiates apoptotic effect of trichostatin A on human epithelial ovarian carcinoma cell lines. Eur J Pharmacol 649**:** 354-361.

Lee MD, Wilson C, Saunter CD, Kennedy C, Girkin JM, & McCarron JG (2018). Spatially structured cell populations process multiple sensory signals in parallel in intact vascular endothelium. Sci Signal 11.

Leybaert L, Lampe PD, Dhein S, Kwak BR, Ferdinandy P, Beyer EC*, et al.* (2017). Connexins in Cardiovascular and Neurovascular Health and Disease: Pharmacological Implications. Pharmacol Rev 69**:** 396-478.

Lin KW, Huang AM, Hour TC, Yang SC, Pu YS, & Lin CN (2011). 18beta-Glycyrrhetinic acid derivatives induced mitochondrial-mediated apoptosis through reactive oxygen species-mediated p53 activation in NTUB1 cells. Bioorg Med Chem 19**:** 4274-4285.

Longden TA, Dabertrand F, Koide M, Gonzales AL, Tykocki NR, Brayden JE*, et al.* (2017). Capillary K+-sensing initiates retrograde hyperpolarization to increase local cerebral blood flow. Nature Neuroscience 20**:** 717-+.

Matchkov VV, Rahman A, Peng H, Nilsson H, & Aalkjaer C (2004). Junctional and nonjunctional effects of heptanol and glycyrrhetinic acid derivates in rat mesenteric small arteries. Br J Pharmacol 142**:** 961-972.

McCarron JG, Chalmers S, MacMillan D, & Olson ML (2010). Agonist-evoked Ca^{2+} wave progression requires Ca^{2+} and IP_3. Journal of Cell Physiology 244**:** 334-344.

McCarron JG, Flynn ER, Bradley KN, & Muir TC (2000). Two Ca^{2+} entry pathways mediate InsP_3-sensitive store refilling in guinea-pig colonic smooth muscle. J Physiol 525 113-124.

McCarron JG, Lee MD, & Wilson C (2017). The Endothelium Solves Problems That Endothelial Cells Do Not Know Exist. Trends Pharmacol Sci 38**:** 322-338.

McCarron JG, & Olson ML (2008). A single luminally continuous sarcoplasmic reticulum with apparently separate Ca^{2+} stores in smooth muscle. J Biol Chem 283**:** 7206-7218.

McCarron JG, Wilson C, Heathcote HR, Zhang X, Buckley C, & Lee MD (2019). Heterogeneity and emergent behaviour in the vascular endothelium. Current opinion in pharmacology 45**:** 23-32.

McGrath JC, & Lilley E (2015). Implementing guidelines on reporting research using animals (ARRIVE etc.): new requirements for publication in BJP. Br J Pharmacol 172**:** 3189-3193.

Morsy MA, Patel SS, El-Sheikh AAK, Savjani JK, Nair AB, Shah JN*, et al.* (2019). Computational and Biological Comparisons of Plant Steroids as Modulators of Inflammation through Interacting with Glucocorticoid Receptor. Mediators Inflamm 2019**:** 3041438.

Narayanan D, Xi Q, Pfeffer LM, & Jaggar JH (2010). Mitochondria control functional CaV1.2 expression in smooth muscle cells of cerebral arteries. Circ Res 107**:** 631-641.

Okamoto T, Akita N, Kawamoto E, Hayashi T, Suzuki K, & Shimaoka M (2014). Endothelial connexin32 enhances angiogenesis by positively regulating tube formation and cell migration. Exp Cell Res 321**:** 133-141.

Olson ML, Chalmers S, & McCarron JG (2010). Mitochondrial Ca^{2+} uptake increases Ca^{2+} release from inositol 1,4,5-trisphosphate receptor clusters in smooth muscle cells. J Biol Chem 285**:** 2040-2050.

Pohl U (2020). Connexins: Key Players in the Control of Vascular Plasticity and Function. Physiol Rev 100**:** 525-572.

Rizzuto R, Brini M, Murgia M, & Pozzan T (1993). Microdomains with high Ca^{2+} close to IP_3-sensitive channels that are sensed by neighboring mitochondria. Science 262**:** 744-747.

Rizzuto R, Pinton P, Carrington W, Fay FS, Fogarty KE, Lifshitz LM*, et al.* (1998). Close contacts with the endoplasmic reticulum as determinants of mitochondrial Ca^{2+} responses. Science 280**:** 1763-1766.

Rouach N, Segal M, Koulakoff A, Giaume C, & Avignone E (2003). Carbenoxolone blockade of neuronal network activity in culture is not mediated by an action on gap junctions. J Physiol 553**:** 729-745.

Saez JC, Berthoud VM, Branes MC, Martinez AD, & Beyer EC (2003). Plasma membrane channels formed by connexins: their regulation and functions. Physiol Rev 83**:** 1359-1400.

Salvi M, Fiore C, Battaglia V, Palermo M, Armanini D, & Toninello A (2005). Carbenoxolone induces oxidative stress in liver mitochondria, which is responsible for transition pore opening. Endocrinology 146**:** 2306-2312.

Schindelin J, Arganda-Carreras I, Frise E, Kaynig V, Longair M, Pietzsch T*, et al.* (2012). Fiji: an open-source platform for biological-image analysis. Nat Methods 9**:** 676-682.

Socha MJ, Domeier TL, Behringer EJ, & Segal SS (2012). Coordination of intercellular Ca^{2+} signaling in endothelial cell tubes of mouse resistance arteries. Microcirculation 19**:** 757-770.

Sonkusare SK, Bonev AD, Ledoux J, Liedtke W, Kotlikoff MI, Heppner TJ*, et al.* (2012). Elementary Ca^{2+} signals through endothelial TRPV4 channels regulate vascular function. Science 336**:** 597-601.

Spray DC, Ye ZC, & Ransom BR (2006). Functional connexin "hemichannels": a critical appraisal. Glia 54**:** 758-773.

Sward K, Dreja K, Lindqvist A, Persson E, & Hellstrand P (2002). Influence of mitochondrial inhibition on global and local $[Ca^{2+}]_i$ in rat tail artery. Circ Res 90**:** 792-799.

Szado T, Kuo KH, Bernard-Helary K, Poburko D, Lee CH, Seow C*, et al.* (2003). Agonist-induced mitochondrial Ca^{2+} transients in smooth muscle. Faseb J 17**:** 28-37.

Tallini YN, Brekke JF, Shui B, Doran R, Hwang SM, Nakai J*, et al.* (2007). Propagated endothelial Ca^{2+} waves and arteriolar dilation in vivo: measurements in Cx40BAC GCaMP2 transgenic mice. Circ Res 101**:** 1300-1309.

Taniguchi Ishikawa E, Gonzalez-Nieto D, Ghiaur G, Dunn SK, Ficker AM, Murali B*, et al.* (2012). Connexin-43 prevents hematopoietic stem cell senescence through transfer of reactive oxygen species to bone marrow stromal cells. Proc Natl Acad Sci U S A 109**:** 9071-9076.

Taylor MS, & Francis M (2014). Decoding dynamic Ca^{2+} signaling in the vascular endothelium. Frontiers in physiology 5**:** 447.

Tran QK, & Watanabe H (2006). Calcium signalling in the endothelium. Handbook of experimental pharmacology**:** 145-187.

Vessey JP, Lalonde MR, Mizan HA, Welch NC, Kelly ME, & Barnes S (2004). Carbenoxolone inhibition of voltage-gated Ca channels and synaptic transmission in the retina. J Neurophysiol 92**:** 1252-1256.

Wang D, Wong HK, Feng YB, & Zhang ZJ (2014). 18beta-glycyrrhetinic acid induces apoptosis in pituitary adenoma cells via ROS/MAPKs-mediated pathway. J Neurooncol 116**:** 221-230.

Willebrords J, Maes M, Crespo Yanguas S, & Vinken M (2017). Inhibitors of connexin and pannexin channels as potential therapeutics. Pharmacol Ther 180**:** 144-160.

Wilson C, Lee M, & McCarron JG (2016a). Acetylcholine released by endothelial cells facilitates flow-mediated dilatation. J Physiol 594**:** 7267–7307.

Wilson C, Lee MD, Heathcote HR, Zhang X, Buckley C, Girkin JM*, et al.* (2019). Mitochondrial ATP production provides long-range control of endothelial inositol trisphosphate-evoked calcium signaling. J Biol Chem 294**:** 737-758.

Wilson C, Lee MD, & McCarron JG (2016b). Acetylcholine released by endothelial cells facilitates flow-mediated dilatation. J Physiol 594**:** 7267-7307.

Wilson C, Saunter CD, Girkin JM, & McCarron JG (2015). Pressure-dependent regulation of Ca^{2+} signaling in the vascular endothelium. J Physiol 593**:** 5231–5253.

Wilson C, Saunter CD, Girkin JM, & McCarron JG (2016). Clusters of specialized detector cells provide sensitive and high fidelity receptor signaling in intact endothelium. Faseb J 30**:** 2000-2013.

Wilson C, Zhang X, Buckley C, Heathcote HR, Lee MD, & McCarron JG (2019). Increased Vascular Contractility in Hypertension Results From Impaired Endothelial Calcium Signaling. Hypertension 74(5)::** 1200-1214.

Yang JC, Myung SC, Kim W, & Lee CS (2012). 18beta-glycyrrhetinic acid potentiates Hsp90 inhibition-induced apoptosis in human epithelial ovarian carcinoma cells via activation of death receptor and mitochondrial pathway. Mol Cell Biochem 370**:** 209-219.

Yu J, Berga SL, Zou W, Sun HY, Johnston-MacAnanny E, Yalcinkaya T*, et al.* (2014). Gap junction blockade induces apoptosis in human endometrial stromal cells. Mol Reprod Dev 81**:** 666-675.

Zhang X, Lee MD, Wilson C, & McCarron JG (2019). Hydrogen peroxide depolarizes mitochondria and inhibits IP3-evoked Ca(2+) release in the endothelium of intact arteries. Cell Calcium 84**:** 102108.